HHS Public Access

Author manuscript

Cell Rep. Author manuscript; available in PMC 2024 March 20.

Published in final edited form as:

Cell Rep. 2024 February 27; 43(2): 113674. doi:10.1016/j.celrep.2024.113674.

Sympathetic NPY controls glucose homeostasis, cold tolerance, and cardiovascular functions in mice

Raniki Kumari[1,5], **Raluca Pascalau**[1,4,5], **Hui Wang**[2], **Sheetal Bajpayi**[3], **Maria Yurgel**[2], **Kwaku Quansah**[1,3], **Samer Hattar**[2], **Emmanouil Tampakakis**[3], **Rejji Kuruvilla**[1,6,*]

[1]Department of Biology, Johns Hopkins University, Baltimore, MD 21218, USA

[2]Section on Light and Circadian Rhythms, National Institute of Mental Health, National Institutes of Health, Bethesda, MD 20892, USA

[3]Division of Cardiology, Johns Hopkins School of Medicine, Baltimore, MD 21205, USA

[4]Present address: Research and Development Institute, Faculty of Medicine, Transylvania University of Brasov, Brasov 500484, Romania

[5]These authors contributed equally

[6]Lead contact

SUMMARY

Neuropeptide Y (NPY) is best known for its effects in the brain as an orexigenic and anxiolytic agent and in reducing energy expenditure. NPY is also co-expressed with norepinephrine (NE) in sympathetic neurons. Although NPY is generally considered to modulate noradrenergic responses, its specific roles in autonomic physiology remain under-appreciated. Here, we show that sympathetic-derived NPY is essential for metabolic and cardiovascular regulation in mice. NPY and NE are co-expressed in 90% of prevertebral sympathetic neurons and only 43% of paravertebral neurons. NPY-expressing neurons primarily innervate blood vessels in peripheral organs. Sympathetic-specific NPY deletion elicits pronounced metabolic and cardiovascular defects in mice, including reductions in insulin secretion, glucose tolerance, cold tolerance, and pupil size and elevated heart rate, while notably, however, basal blood pressure was unchanged. These findings provide insight into target tissue-specific functions of NPY derived from sympathetic neurons and imply its potential involvement in metabolic and cardiovascular diseases.

*Correspondence: rkuruvilla@jhu.edu.

AUTHOR CONTRIBUTIONS

R.P., R. Kumari, and R. Kuruvilla designed the study. R.P. and R. Kumari conducted the majority of the experiments and analyzed data. H.W., M.Y., and S.H. provided guidance with pupil analyses and temperature recordings. K.Q. assisted with whole-organ immunohistochemistry. S.B. and E.T. performed the heart rate and blood pressure analyses. R.P., R. Kumari, and R. Kuruvilla wrote the manuscript.

DECLARATION OF INTERESTS

The authors declare no competing interests.

SUPPLEMENTAL INFORMATION

Supplemental information can be found online at https://doi.org/10.1016/j.celrep.2024.113674.

In brief

Using intersectional genetic labeling and conditional knockout mice, Kumari et al. describe the differential expression of NPY between prevertebral and paravertebral sympathetic ganglia and reveal specific roles for peripheral sympathetic-derived NPY in regulating autonomic physiology, including cardiovascular function, blood glucose homeostasis, cold tolerance, and pupil size.

Graphical Abstract

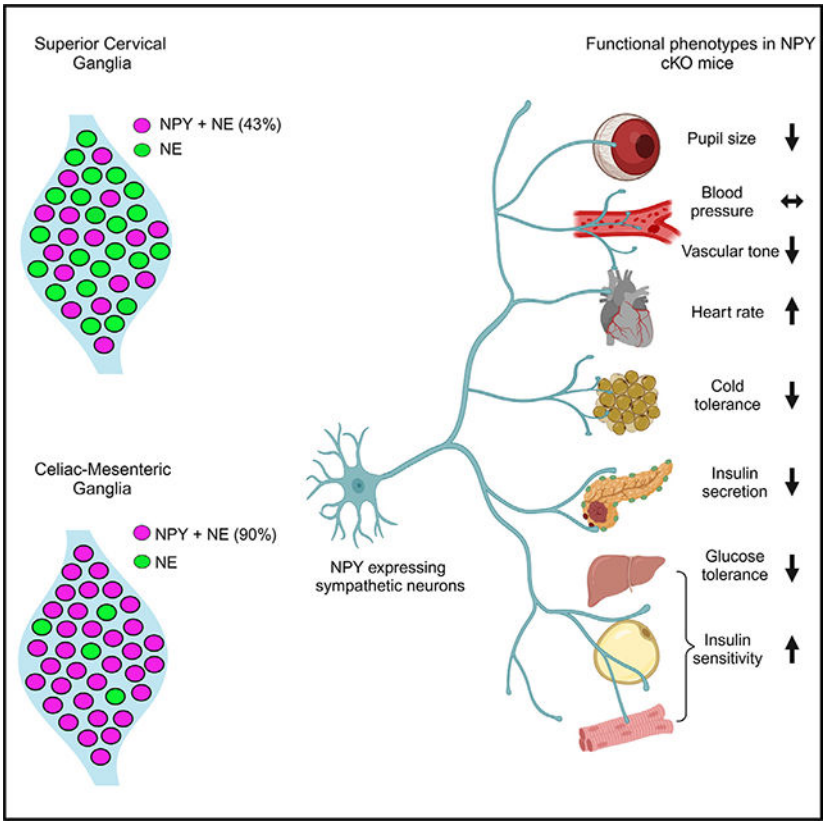

INTRODUCTION

The sympathetic nervous system is a major conduit for communication between the brain and the periphery. While widely known for its role in triggering “fight-or-flight responses” in the event of danger or stress, the sympathetic nervous system is also vital for maintaining body homeostasis during daily activities such as feeding or exercising. Organized into a system of ganglia and nerves in the peripheral nervous system (PNS), sympathetic neuron cell bodies, resident in ganglia, send long axonal projections throughout the body to innervate diverse peripheral organs and tissues to control a broad spectrum of physiological processes including heart rate, blood pressure, body temperature, blood glucose levels, and immune function.[1] Homeostatic and adaptive sympathetic regulation of different peripheral organs is remarkably precise, suggesting the existence of dedicated neural circuits that drive different effector organ functions.[2] However, there is limited understanding of the functional diversity of sympathetic neurons at the molecular and cellular levels.

It has been proposed that one basis for the functional diversity of sympathetic neurons is the combinatorial expression of neuropeptides along with a classical neurotransmitter, which provides a “neurochemical code” that allows for the innervation of distinct target organs and the regulation of specific autonomic functions.[3] Neuropeptide Y (NPY) is a 36-amino-acid peptide that is co-stored and co-released with norepinephrine (NE) from sympathetic neurons and adrenal glands.[4–7] In contrast to the vast amount of knowledge of the potent effects of NPY expressed in brain regions, specifically hypothalamic and brainstem nuclei in regulating food intake,[8,9] mood,[10] energy balance,[11] and cardiovascular functions,[12,13] the actions of NPY in peripheral sympathetic neurons have been relatively under-studied. NPY functions have been largely studied at the whole-organism level using global knockout mice[11,14–17] or by pharmacological manipulations,[18] and the knowledge of specific roles for NPY in defined neuronal populations remains incomplete.

In sympathetic neurons, electrophysiological and pharmacological studies on tissue preparations indicate that NPY is co-released with NE from nerve terminals, specifically during prolonged or high-frequency stimulation.[4] Sympathetic-derived NPY has mild vasoconstrictor effects on its own,[5,6] although it powerfully potentiates NE-induced vascular contractile responses by acting postsynaptically.[5,19–22] NPY, released from sympathetic nerves, also exerts a presynaptic effect in inhibiting NE release.[21,23] More recent studies with genetic ablation of NPY and NE co-expressing sympathetic neurons suggest roles for these neurons in modulating inflammatory responses[24] and cardiac excitability[25] in mice. However, whether observed phenotypes were due to the loss of NPY, NE, or other neuron-derived factors could not be delineated from these studies. Thus, other than its classical role as a modulator of sympathetic neurotransmission, the specific functions of NPY expressed in sympathetic neurons remain to be elucidated.

Here, using an intersectional genetic labeling approach, we show that sympathetic neurons co-expressing NPY and NE are more abundant in prevertebral, compared to paravertebral, sympathetic ganglia. Axons of NPY and NE co-expressing sympathetic neurons extend along, and primarily innervate, blood vessels in peripheral tissues. Using conditional knockout mice, we show that loss of NPY from sympathetic neurons does not affect neuron development, target innervation, or activity but does result in pronounced metabolic and cardiovascular defects, including reductions in insulin secretion, glucose tolerance, cold tolerance, and pupil size and an elevation in heart rate. Surprisingly, despite the well-documented role of NPY in vasoconstriction, we found that blood pressure under basal conditions was unaffected in mutant mice. We also found elevated circulating NE levels in NPY conditional knockout mice, which may be due, in part, to increased NE biosynthesis in adrenal glands. Together, these findings provide fresh insight into specific actions of NPY in the sympathetic nervous system.

RESULTS

NPY is expressed in a higher proportion of sympathetic neurons in prevertebral ganglia

Anatomically, the sympathetic nervous system is organized into paired paravertebral ganglia located in chains along the rostro-caudal axis on both sides of the spinal cord, and single prevertebral ganglia located at the midline, ventral to the spinal cord. Although

NPY is widely considered to be a co-transmitter with NE in sympathetic neurons,[22] previous studies have suggested that NPY expression is not uniform among noradrenergic sympathetic neuron populations.[26–28] Here, we used a genetic labeling approach to assess the distribution of NPY-expressing sympathetic neurons. *NPY*^{Cre} mice[29] were crossed with *ROSA26*^{eYFP} mice[30] in conjunction with immunostaining for tyrosine hydroxylase (TH) to mark noradrenergic neurons. We chose the superior cervical ganglia (SCGs), the rostral-most ganglia in the sympathetic chain, and the celiac-superior mesenteric ganglia (CG-SMGs), which lie within the abdominal cavity, to represent para- and prevertebral ganglia, respectively. SCG neurons project to the head and neck vasculature, eye, pineal glands, salivary glands, and skin overlying the head and neck, while CG-SMG neurons project to abdominal organs including liver, pancreas, spleen, kidneys, stomach, and the proximal small intestine.

We found that ~90% of TH-positive sympathetic neurons expressed the EYFP reporter in CG-SMGs (Figures 1B and 1F) compared to only ~43% in the SCGs in postnatal day 21 mice (Figures 1A and 1E). Since the genetic reporter labels all cells that expressed *Npy* at any moment during development, including any that may have subsequently down-regulated NPY protein expression, we also performed NPY immunostaining. Similar to observations with genetic labeling, the majority of TH-positive neurons showed NPY immunoreactivity in the CG-SMGs compared to partial overlap in the SCGs at postnatal day 21 (Figures 1C and 1D). Quantification revealed that 25% of TH-positive neurons were GFP^{+};NPY^{-} in the SCGs compared to 6.3% in the CG-SMGs, suggesting that NPY protein expression is down-regulated in a significant proportion of sympathetic neurons in the SCG but not in the CG-SMG.

To examine changes in the proportion of NPY-expressing neurons in sympathetic ganglia over time, we performed genetic and immunofluorescence labeling at various developmental time points in mice. We found that the percentage of NPY-immunoreactive (GFP^{+};NPY^{+}) noradrenergic neurons (~90%) remains constant across all developmental time points examined (embryonic day 15, postnatal days 1, 7, 14, and P21) in the CG-SMG (Figure 1F). In contrast, in the SCG, the percentage of NPY-expressing sympathetic neurons decreases from 65% at embryonic day 15 (E15) to 41% at postnatal day 7 (P7) and then stays constant at the later postnatal stages examined (P14 and P21) (Figure 1E). The decrease in the NPY-immunoreactive population in the SCG is likely due to down-regulation of NPY expression and not cell loss, as the percentage of genetically labeled neurons (GFP-positive) remained largely unchanged over time (Figure 1E). Further, of note, almost one-third (32%) of TH-positive neurons in the SCG were neither NPY nor GFP positive when examined at P21, while this population was minimal (3.6%) in the CG-SMG (Figures 1E and 1F).

Together, these results indicate that the proportion of NPY-expressing noradrenergic neurons is markedly higher in pre- vs. paravertebral sympathetic ganglia. Further, in prevertebral neurons, the adult pattern of NPY and NE co-expressing neurons is acquired early at embryonic stages and maintained throughout development compared to paravertebral neurons, where the mature pattern of NPY expression is only established after birth.

NPY-expressing sympathetic axons largely innervate blood vessels

Given the differential abundance of NPY-expressing neurons in para- and prevertebral sympathetic ganglia, we next wanted to define their axonal projections to diverse peripheral organs and tissues. NPY is expressed in many non-neuronal cells in peripheral tissues, including blood platelets,[31] white adipose tissue,[32] bone cells,[33] and pancreatic beta cells,[34] which would have been labeled by the NPY^{Cre};$ROSA26^{EYFP}$ reporter mice or by NPY immunostaining (see Figure S1A), making it difficult to distinguish the signal coming from innervating axons. To specifically visualize NPY-expressing sympathetic nerves, we used an intersectional genetic approach. We crossed a dual-recombinase-dependent reporter mouse line, $Rosa26^{LSL\text{-}FSF\text{-}tdTomato}$ *(Ai65)* mice,[35] to DBH^{Cre}[36] and NPY^{FLP} mice[37] (Figure 2A). In DBH^{Cre};NPY^{FLP};$ROSA26^{LSL\text{-}FSF\text{-}tdTomato}$ mice (henceforth referred to as NPY^{DBH}-*TdTomato* mice), tdTomato reporter expression is restricted to NPY^{DBH} sympathetic neurons co-expressing NPY and dopamine beta-hydroxylase (DBH), an enzyme in the NE biosynthetic pathway.

We observed NPY reporter expression in paravertebral sympathetic chain ganglia distributed along the rostro-caudal axis in postnatal (P6) mice as visualized by whole-mount TH and red fluorescent protein (RFP) immunostaining and light-sheet microscopy (Figure 2B). Similar to the observations in NPY^{Cre};$ROSA26^{EYFP}$ mice, reporter expression showed partial overlap with TH immunoreactivity in paravertebral ganglia (SCGs) and almost complete overlap with TH in prevertebral ganglia (CG-SMGs) in NPY^{DBH}-*TdTomato* mice (Figures 2C and 2D).

To visualize innervation of peripheral organs by NPY-expressing sympathetic axons, we performed immunostaining using antibodies against tdTomato, TH, or NPY in tissue sections or whole-mounts from NPY^{DBH}-*TdTomato* mice at postnatal day 6. In salivary glands and interscapular brown adipose tissue (BAT), which are innervated by paravertebral ganglia neurons in the SCG and by stellate/thoracic chain ganglia, respectively, we observed tdTomato reporter expression in axons extending along blood vessels and also in finer branches within the tissue parenchyma (Figures 2E and 2F). However, compared to reporter expression, NPY immunoreactivity was only present in axons associated with blood vessels (Figures 2E and 2F). These results suggest that the developmental down-regulation of NPY expression specifically occurs in neurons that innervate the tissue parenchyma and that vascular-derived signals may be required for the maintenance of NPY expression in sympathetic neurons. We cannot exclude the possibility, however, that axons innervating the tissue parenchyma and blood vessels are derived from the same neurons and that NPY is specifically down-regulated locally in the collaterals innervating non-vascular targets. TH immunostaining showed partial co-localization of TH immunoreactivity with reporter signal in axons innervating salivary glands and BAT (Figures S1B and S1C), consistent with the pattern of co-expression of TH and NPY in neuronal cell bodies in paravertebral ganglia at postnatal stages.

For prevertebral targets, we assessed innervation of the mesenteric artery, a major artery supplying the gastrointestinal tract, as well as the pancreas, which receives innervation from CG-SMG neurons.[38] tdTomato labeling showed a dense meshwork of NPY-expressing fibers around the mesenteric artery and aligned along smaller blood vessels in the pancreas

(Figures 2G and S1A). NPY protein expression largely overlaps with tdTomato reporter signal (Figures 2G and S1A), as well as with TH immunoreactivity (Figures S1D and S1E), consistent with the observations that the majority of prevertebral ganglia neurons co-express NPY and TH and that NPY protein expression is not down-regulated during development as in the paravertebral ganglia.

In addition to sympathetic neurons, NPY is also expressed in adrenal chromaffin cells,[39–41] which are neuroendocrine cells that primarily secrete epinephrine, but also NE, to regulate myriad cardiovascular and metabolic processes, particularly in response to stressful stimuli. Similar to prevertebral neurons, we also observed a complete overlap between tdTomato reporter expression, NPY, and TH immunostaining in adrenal chromaffin cells in *NPY*$^{DBH\text{-}TdTomato}$ mice at postnatal day 6 (Figures 2H and S1F). These results suggest that the developmental regulation of NPY expression in adrenal glands resembles the scenario in prevertebral ganglia neurons.

Together, these results suggest that NPY-expressing sympathetic neurons largely associate with blood vessels in peripheral target tissues that are innervated by both pre- and paravertebral ganglia neurons. However, the majority of axons from prevertebral noradrenergic neurons maintain NPY expression during postnatal life compared to paravertebral neurons, consistent with the patterns observed in neuronal cell bodies.

Loss of sympathetic NPY elicits soma atrophy but does not affect neuron survival or target innervation

To address the function(s) of NPY in sympathetic neurons, we generated conditional knockout mice, where mice with a floxed *NPY* allele (*NPY*$^{fl/fl}$ mice)[42] were crossed with *DBH*^{Cre} mice. *DBH*^{Cre};*NPY*$^{fl/fl}$ mice (henceforth referred to as NPY cKO [conditional knockout] mice) survived to adulthood, had no gross morphological abnormalities, and had normal body weight (see Figure 5A). Littermate *NPY*$^{fl/fl}$ mice were used as controls in all analyses. NPY expression, visualized by immunofluorescence, was significantly reduced in mutant sympathetic (CG-SMG) ganglia (Figure 3A), and quantitative PCR (qPCR) analysis indicated an almost complete loss of *Npy* transcript in paravertebral (SCG) and prevertebral (CG-SMG) ganglia (Figure 3B). Given that adrenal chromaffin cells also co-express DBH and NPY,[41] we saw a drastic reduction in *Npy* mRNA levels in adrenal glands in mutant mice (Figure 3B).

To ask if loss of NPY in sympathetic neurons affects their development, we visualized neuron morphology using TH immunostaining and quantified neuron numbers in sympathetic ganglia using Nissl staining in mice at P21. Loss of NPY had no effect on TH expression in sympathetic neurons (Figure 3C) but elicited a marked atrophy of neuronal soma (Figures 3D and 3E). Soma areas from tissue sections were 258 ± 8 μm^2 for control neurons vs. 184 ± 10 μm^2 for mutant neurons. Soma size has been postulated to correlate with increased translational and metabolic machinery in neurons,[43–45] suggesting that NPY may be required for these biochemical functions in sympathetic neurons. Despite the soma atrophy, sympathetic neuron numbers were not significantly different from that in control littermates (4,324 ± 455 in control vs. 4,484 ± 539.5 in mutant mice) based on quantification of cell counts (Figures 3F and 3G). Given the higher proportion of NPY and

NE-co-expressing neurons in the CG-SMG, we largely focused on these ganglia, although similar results were obtained in the SCG. Whole-organ TH immunostaining in iDISCO-cleared tissues and light-sheet microscopy showed that axon innervation density in diverse target tissues including the heart and BAT (paravertebral targets) as well as mesenteric arteries and kidney (prevertebral targets) were unaffected in NPY cKO mice (Figures 3H–3K).

Together, these results indicate that NPY regulates sympathetic neuron soma size but is dispensable for neuron survival and target innervation during development.

NPY cKO mice have elevated circulating NE levels

Previous studies have documented that central NPY signaling suppresses sympathetic tone,[46–48] while NPY, derived from peripheral sources, exerts post- and presynaptic effects in potentiating NE-induced responses and inhibiting NE release, respectively.[21,49,50] To address how the selective loss of NPY in sympathetic neurons affects neuron activity, we performed immunostaining for c-Fos, an immediate-early transcription factor that serves as a reporter of neuronal activity,[51] in CG-SMG tissue sections. We found similar numbers of c-Fos-positive sympathetic neurons in control and NPY cKO mice (11.2 ± 1.0 in control vs. 9.33 ± 1.3 in mutant) at room temperature (Figures 4A–4C and 4E). Activation of the sympathetic nervous system by a brief (1 h) cold exposure at 4°C significantly increased the number of c-Fos-positive cells by ~4.7- to 6.2-fold in both control and mutant ganglia (53.0 ± 2.6 in control vs. 57.6 ± 4.0 in mutant) (Figures 4B–4D and 4E). These results suggest that basal and cold-induced activity in sympathetic ganglia is not affected by the loss of NPY.

To address the effects of NPY loss in sympathetic neurons on NE release, we measured circulating NE levels in NPY cKO and control mice kept at room temperature or exposed to 4°C for 2 h. Plasma NE levels are thought to be primarily derived from sympathetic nerves, although a smaller contribution comes from secretion from adrenal chromaffin cells.[52] At room temperature, we observed a significant increase (2.2-fold) in circulating NE in mutant mice compared to control animals (Figure 4F). In control animals, cold exposure at 4°C significantly increased plasma NE compared to room temperature (Figure 4F), consistent with elevated sympathetic activity. However, in NPY cKO animals, there was no further elevation in plasma NE in response to cold exposure (Figure 4F).

In addition to regulating NE release, NPY signaling has also been reported to regulate NE biosynthesis.[53] qPCR analyses showed that expression of *Th*, the rate-limiting enzyme in NE synthesis, was unaffected in sympathetic ganglia from NPY cKO mice (Figure 4G), However, there was a significant up-regulation of TH expression in adrenal glands from NPY cKO mice, as revealed by qPCR and immunostaining (Figures 4G and 4H). These results are consistent with previous studies using global deletion of NPY or its receptor Y1 or pharmacological Y1R inhibition, where NPY was found to decrease TH expression in adrenal glands.[53,54]

Together, these results suggest that under basal conditions, NPY acts to lower NE release through presynaptic inhibition in sympathetic nerve terminals and/or blunts NE synthesis

in adrenal glands to keep the circulating NE levels low, so that NE levels only increase in specific situations when a heightened sympathetic response is required.

Loss of sympathetic NPY elicits pronounced metabolic and cardiovascular defects in mice

To address the functional consequences of loss of sympathetic-derived NPY, we performed a battery of physiological analyses in NPY cKO mice and control littermates. In contrast to the effects of manipulating central NPY signaling that alter body weight and food intake,[9,11,55] selective deletion of NPY from peripheral sympathetic neurons had no effect on these parameters when assessed in 1-month-old mice (Figures 5A and 5B).

Blood pressure is a function of vascular resistance and cardiac output, which are both controlled by the sympathetic nervous system.[56] Since NPY has been reported to be a potent vasoconstrictor, either acting directly[5,6] or potentiating the effects of NE,[20–22] we expected that loss of sympathetic NPY would result in a drop in blood pressure. Further, NPY administration in humans[57] or its over-expression in animals results in a long-lasting increase in blood pressure.[58] However, we found that resting systolic and diastolic blood pressures were not changed in NPY cKO mice when measuring arterial blood pressure in resting, unrestrained, and conscious mice (Figure 5C). In contrast to normal blood pressure, we observed a striking increase in heart rate in NPY cKO mice compared to control littermates, as assessed by electrocardiographic (ECG) recordings (Figures 5D and 5E). Thus, increased cardiac output might serve as a counter-acting adaptive mechanism to mask any drop in blood pressure in the absence of the vasoconstrictor effects of sympathetic-derived NPY.

The sympathetic nervous system is a key contributor to the control of glucose homeostasis.[38,59] Sympathetic nerve-derived NE signaling rapidly elevates blood glucose levels, necessary in fight-or-flight situations, by decreasing pancreatic insulin secretion and peripheral insulin sensitivity and by increasing pancreatic glucagon secretion.[59] NPY administration to isolated pancreas/islets inhibits insulin secretion,[60] while global NPY KO mice show elevated insulin secretion,[61] suggesting that it acts to potentiate NE effects. To address the role of sympathetic-derived NPY in insulin secretion, we assessed glucose-stimulated insulin secretion in NPY cKO and control mice *in vivo*. Unexpectedly, NPY cKO mice showed a pronounced reduction in plasma insulin levels in response to a glucose challenge compared to control animals (Figure 5F). To address whether the altered insulin secretion in NPY cKO mice was an islet-intrinsic defect, we isolated islets from control and NPY cKO mice and measured basal insulin secretion (in response to 2.8 mM glucose) and also induced by high glucose (16.7 mM). We found that glucose-stimulated insulin secretion was completely abolished in NPY cKO islets (Figure 5G), although basal insulin secretion and total insulin content were not affected (Figures 5G and S2A). The observations in isolated islets from NPY cKO mice suggest that loss of sympathetic-nerve-derived NPY results in islet-intrinsic changes that then attenuate insulin secretion. Of note, NPY expression is down-regulated in mature islets,[34,62] and DBH is not expressed in islet cells (see Figure S1A), suggesting that the insulin secretion defect in NPY cKO islets is not due to NPY loss in islet cell types. In contrast to insulin secretion, circulating glucagon levels in response to insulin-induced hypoglycemia were unaffected in NPY cKO animals

(Figure S2B). Consistent with the blunted insulin secretion in NPY cKO mice, we found that mutant mice had impaired glucose tolerance compared to control animals (Figure 5H). However, the glucose intolerance was milder than expected from the striking decrease in glucose-stimulated insulin secretion *in vivo* and *in vitro*. One potential explanation is that we found that NPY cKO mice showed improved insulin sensitivity compared to control littermates (Figure 5I). Since glucose tolerance is determined by both insulin secretion and sensitivity, the reduced insulin secretion in mutant mice is balanced by the increased sensitivity of insulin-responsive peripheral tissues such as muscle, liver, and adipose tissue. Together, these results reveal that sympathetic-derived NPY controls glucose homeostasis, in part, by positively regulating islet insulin secretion. Further, the improved insulin sensitivity in NPY cKO animals may reflect a compensatory response to the low plasma insulin levels and/or a decrease in noradrenergic signaling in insulin-responsive peripheral organs, including liver, adipose tissue, and striated muscles, in the absence of sympathetic NPY.

The sympathetic nervous system is a critical mediator of physiological responses to cold exposure through triggering piloerection, vasoconstriction, and non-shivering thermogenesis in the BAT.[63] To address if NPY expressed in sympathetic neurons is required to maintain body temperature in response to cold exposure, we performed a cold tolerance test in NPY cKO and control animals. Mice were implanted with subcutaneous temperature sensors, and body temperatures were first recorded at room temperature, following which mice were moved to 4°C and body temperatures measured every 15 min for 4 h. While both NPY cKO and control animals were able to maintain their internal temperatures for the first hour at 4°C, the body temperatures in mutant mice dropped sharply compared to the controls with prolonged cold exposure (Figure 5J). Thus, sympathetic-derived NPY is required for animals to mount appropriate physiological responses to cold. Together with our observations that NPY cKO animals fail to show an increment in circulating NE in response to a brief cold stimulus (4°C, 2 h) (Figure 4F), these results suggest that stress-induced responses are impaired in mutant animals.

Lastly, we assessed pupil size, which is controlled by a balance between the pupil dilator muscle, innervated by sympathetic fibers from the SCG, and the pupillary sphincter muscle, innervated by parasympathetic nerves coming from the ciliary ganglion.[64] Sympathetic-nerve-derived NE signaling drives the contraction of smooth muscle cells in dilator muscle.[64] To measure basal pupil size, control and NPY cKO mice were dark adapted for over 2 h, and pupil sizes were recorded for 10 s in the dark under non-anesthetized conditions. We observed decreased basal pupil areas in NPY cKO mice compared to controls (Figures 5K and S2C). To ask whether this phenotype is due to decreased parasympathetic activity, we measured pupil constriction in response to increasing light intensities, ranging from 0.01 to 1000 lux, administered for 30 s. Light onset at 0.1 lux or higher resulted in rapid constriction with greater constrictions at higher light intensities in both NPY cKO and control mice (Figure S2D). The intensity responses were virtually identical for the two groups (Figure S2D). These results suggest that parasympathetic function is intact in NPY cKO mice and that the decreased pupil areas likely reflect reduced noradrenergic signaling at the pupil dilator muscle with the loss of sympathetic-derived NPY.

DISCUSSION

Despite decades of research on NPY, specifically for its actions in the brain, the peripherally mediated functions of NPY have remained relatively under-appreciated. Here, using cKO mice, we reveal specific roles for NPY expressed in peripheral sympathetic neurons in controlling neuron soma size during development and in regulating autonomic physiology, including cardiovascular function, blood glucose homeostasis, cold tolerance, and pupil size, in adult animals.

In contrast to the canonical view that NPY primarily functions as a modulator of sympathetic neurotransmission,[65,66] our results suggest a more complex scenario. For example, NPY cKO mice showed decreased glucose-stimulated insulin secretion and impaired glucose tolerance (Figures 5F–5H), which is contrary to that predicted from the loss of NPY-mediated potentiation of NE signaling, where NE is known to potently inhibit insulin secretion and elevate blood glucose.[38] Strikingly, the phenotypes in NPY cKO mice recapitulate the effects that we previously observed with developmental ablation of sympathetic nerves,[67] which resulted in reduced insulin secretion and glucose intolerance as well as disruptions in islet architecture in mice.[67] Since NPY is removed early during embryonic development in NPY cKO mice, these findings suggest that nerve-derived NPY might exert a developmental role in regulating islet morphology and function. Unexpectedly, we also observed an increase in heart rate in NPY cKO animals, which, at first glance, was incongruent with a canonical function for NPY in potentiating NE effects. However, given the normal blood pressure in NPY cKO mice, we reason that the increased heart rate may be due to a compensatory cardiac self-regulatory response aimed to maintain the blood pressure constant in a condition of low vascular resistance when NPY is removed from sympathetic nerves. Alternatively, the elevated heart rate in mutant animals could reflect a direct role for sympathetic-derived NPY in reducing heart rate through inhibition of parasympathetic cholinergic signaling.[68] Other phenotypes observed in NPY cKO mice, for example the improved insulin insensitivity, impaired cold tolerance, and reduced basal pupil size, are all consistent with decreased sympathetic tone and the reported canonical role of NPY in potentiating NE signaling. Together, our results suggest that NPY derived from sympathetic neurons can act alone or in concert with the classical neurotransmitter, NE, in a target-tissue-dependent context.

We found that NPY is expressed in a substantially higher proportion (90%) of sympathetic neurons in prevertebral compared to paravertebral ganglia (43%). It has been proposed that paravertebral ganglion neurons serve as a “simple” direct relay for fast transmission of information from the CNS to the targets.[69] In contrast, prevertebral neurons integrate multiple inputs including those coming from preganglionic neurons, collaterals of visceral primary afferent neurons with cell bodies in dorsal root ganglia, and intestinofugal neurons of the enteric nervous system.[69] Given that prevertebral neurons depend on spatial and temporal integration of multiple presynaptic inputs, it is possible that NPY-mediated modulation provides greater flexibility and robustness to synaptic transmission from prevertebral compared to paravertebral neurons. Prevertebral neurons also predominantly innervate visceral organs to regulate gastrointestinal motility, secretion, absorption, and blood flow, while paravertebral sympathetic neurons innervate a broad spectrum of

effector organs with much more diverse functions, including pupil dilation, melatonin production, vasoconstriction, salivary and sweat gland secretion, heart rate and contractility, thermoregulation, and respiration. Thus, paravertebral ganglion neurons may be much more diverse with respect to neuropeptide expression compared to prevertebral neurons, to accommodate the greater functional diversity.

We also found that NPY protein expression is down-regulated in a significant proportion (~25%) of paravertebral sympathetic neurons in the postnatal SCG at P7 compared to embryonic stages (E15). In mice, the first week of birth corresponds to the peak period of innervation of target tissues by SCG neurons.[1] It is possible that NPY expression in the neonatal SCG is linked to target-derived signals that either instruct NPY down-regulation or maintain expression. Our results using intersectional genetic labeling and NPY immunostaining suggest that the developmental down-regulation of NPY specifically occurs in neurons that innervate the tissue parenchyma, while NPY expression is maintained in neurons that innervate blood vessels. Previous work also supports that NPY expression is specifically maintained in sympathetic neurons that are cultured in the presence of conditioned media from vascular cells.[70] Thus, the dynamic expression of NPY in developing SCG neurons might be dictated by interactions with target tissues such that neurons innervating vascular targets keep expressing NPY, while axons reaching non-vascular targets either receive no such signals or receive negative signals for NPY down-regulation. The first week of birth also coincides with an increase in the number of synapses between pre- and postganglionic neurons in the SCG.[71] Thus, NPY down-regulation in the P7 SCG may also be linked to local signals within the ganglia, specifically increased preganglionic input and, thereby, neuronal activity.

Axonal terminations of NPY-expressing sympathetic neurons contain small NE-containing vesicles, which are rapidly released upon acute stimulation, as well as large dense core vesicles containing both NE and NPY that slowly release both molecules under prolonged or high-frequency stimulation.[4,72] The finding that NPY is specifically released during intense and prolonged high-frequency activation has led to the view that NPY is poised to regulate sympathetic responses in extreme physiological circumstances, including chronic stress, exposure to danger, and pathological conditions such as heart failure and insulin-induced hypoglycemia.[12,58,73] Yet, we found that loss of NPY from sympathetic neurons results in pronounced autonomic defects, including increased heart rate, impaired insulin secretion, glucose intolerance, and reduced pupil size, under basal conditions. These results reveal that, even under basal conditions, sympathetic-derived NPY exerts a wide range of physiological effects across a number of organ systems. It is possible that under basal conditions, an increase in circulating NE in the absence of sympathetic-derived NPY contributes to some of the phenotypes that we observed in the mutant mice. Together with previous studies, our results suggest that co-existence of NPY with NE in sympathetic nerve terminals and adrenal glands may serve as a buffer to protect tissues from the adverse effects of excessive or chronic NE release.

The NPY system has been widely recognized as one of the most important regulators of whole-body physiology in animals. Yet, despite decades of study, dissecting the tissue- and cell-specific roles of NPY *in vivo* through the use of genetic tools has lagged behind.

Here, through selective deletion of NPY from peripheral sympathetic neurons, we provide direct evidence that sympathetic-derived NPY is essential for metabolic and cardiovascular regulation in mice. There are six classes (Y1–Y6) of NPY receptors, which are G-protein-coupled receptors, that are differentially expressed in several target organs including smooth muscles (Y1), the cardiovascular system (Y1, Y2, Y3, Y5), kidneys (Y1, Y2, Y5, Y6), and gastrointestinal tract (Y1, Y2, Y4), as well in sympathetic axons (Y2).[16,25,46,73,74] In future studies, it will be of interest to use cKO mice to define the specific NPY receptor(s) that mediates effects of sympathetic-neuron-derived NPY in distinct effector organs. In humans, increased circulating NPY has been documented in several pathological conditions in which sympathetic output is also increased, such as hypertension, chronic heart failure, and insulin resistance.[12,75,76] Our findings suggest that targeting peripheral NPY signaling with specific agonists or antagonists can offer possibilities in the treatment of metabolic and cardiovascular diseases.

Limitations of the study

NPY and NE are co-expressed in the nucleus of the solitary tract (NTS)[77,78] and the A1/C1 cluster of catecholaminergic neurons in the brainstem,[27,79] which have been implicated in regulating food intake[77,80] and sympathetic outflow to the periphery.[81,82] While we cannot exclude the possibility that loss of NPY in these brain nuclei may account for some of the phenotypes that we observed in NPY cKO mice, our results suggest that preganglionic input to sympathetic ganglia neurons was unaffected based on c-Fos immunostaining (Figures 4A–4D) and expression of catecholamine synthesizing enzymes such as TH (Figure 4G). Further, food intake was normal in mutant animals. However, additional studies are warranted to fully dissect the roles of NPY and NE co-transmission in the brain vs. periphery. Further, while we used *DBH*^{Cre} mice in this study, the use of viral transduction approaches or tamoxifen-inducible CreERT2 mice for temporal deletion of sympathetic-derived NPY will be important to resolve developmental vs. adult functions.

STAR★METHODS

RESOURCE AVAILABILITY

Lead contact—Further information and requests for resources and reagents should be directed to and will be fulfilled by the lead contact, Rejji Kuruvilla (rkuruvilla@jhu.edu).

Materials availability—All transgenic mice generated in this study (see key resources table) are available upon request.

Data and code availability

- The microscopy and physiological analyses data reported in this paper will be shared by the lead contact upon request.
- This paper does not report original code.
- Any additional information required to re-analyze the data reported in this paper is available from the lead contact upon request.

EXPERIMENTAL MODEL AND SUBJECT DETAILS

Animals—All animal care and experimental procedures were conducted in accordance with the Johns Hopkins University Animal Care and Use Committee (ACUC) and NIH guidelines. All efforts were made to minimize the pain and number of animals used. Animals were group housed in a standard 12:12 light-dark cycle, except for pupil analysis where the animals were dark-adapted for two days, with excess water and food *ad libitum*. The ages of mice are indicated in the figure legends and/or methods. Both male and female mice were used for the analysis. The following lines were used in this study: *NPY*^{Cre} *(B6.Cg-Npytm1(cre)Zman/J,* JAX #027851*)*, *ROSA26*^{eYFP} *(B6.129X1-Gt(ROSA)26Sortm1(EYFP)Cos/J,* JAX #006148*)*, *NPY-Flp (B6.Cg-Npytm1.1(flpo)Hze/J,* JAX #030211*)*, and *ROSA26*^{tdTomato} *(B6;129S-Gt(ROSA)26Sortm65.1(CAG-tdTomato)Hze/J* JAX #021875*)* mice were all obtained from The Jackson Laboratory. *DBH*^{Cre} and *NPY*$^{fl/fl}$ mice were generous gifts from Dr Warren G. Tourtellotte (Northwestern University) and Dr. Ivo Kalajzic (UConn Health), respectively.

METHOD DETAILS

Isolation of RNA and quantitative RT-PCR analysis—Total RNA was isolated from dissected SCG, CG-SMG, and adrenal glands using the TRIzol-chloroform extraction method. cDNA was prepared using Superscript IV First-Strand Synthesis System. Real-time qPCR analysis was performed using a Maxima SYBR green/Rox Q-PCR Master Mix (Thermo Fisher Scientific) and gene-specific primers, in a 7300 real-time PCR system (Applied Biosystem). All samples were analyzed in triplicate reactions. Fold change was calculated using the $2^{(\Delta\Delta Ct)}$ normalized to 18S transcript. Primer sequences are listed in the key resources table.

Food intake—Mice (4–5 weeks) were weighed and then individually housed for a total of 7 days. 100gm of food *ad libitum* was given to each mouse on the first day. The uneaten food was measured each day, total food intake was calculated and normalized to the body weight per mouse.

Norepinephrine (NE) ELISA—Blood samples (300 μL) were drawn retro-orbitally from anesthetized mice (6 weeks) that were either housed at room temperature or exposed to cold (4°C, 2 h). Plasma was prepared by centrifuging blood at 3000 rpm for 15 min, 4°C, and 100 μL plasma was used for NE measurements using ELISA (NE High Sensitive ELISA Kit, Rocky Mountain Diagnostics) according to manufacturer's protocol.

Blood pressure recordings—Blood pressure was measured by a non-invasive system (BP-2000 Series II, Visitech systems). Mice (6–8 weeks) were acclimatized to the machine for two days prior to blood pressure recordings to minimize stress. Each mouse was placed inside a magnetic restrainer and an inflatable occlusion cuff with a light sensor that was passed through the tail. Systolic and diastolic blood pressures were calculated based on the variations in the amount of light transmitted through the tail. 20 blood pressure recordings were averaged to obtain the final measurements for each mouse.

Electrocardiograms—ECG recordings were performed on adult mice.[83] Briefly, mice (6–8 weeks) were anesthetized with 4% isoflurane, intubated, and placed on ventilator support (settings 1.2 mL/g/min at 80 breaths/min). The animal's abdomen was shaved, scrubbed with betadine and alcohol, and draped with a sterile barrier with the surgery site exposed. A small 0.5 cm midline incision was performed and a telemetry unit (DSI Harvard Bioscience Inc.) was implanted intraperitoneally. ECG leads were implanted subcutaneously and sutured over the right upper and left lower chest. Body temperature was maintained at 37°C. Immediately following implantation, the wound was closed with a 3–0 silk suture. Anesthesia was turned off and the animal was monitored for spontaneous breathing and was given a subcutaneous buprenorphine injection (0.01–0.05 mg/kg buprenorphine, IM) to alleviate pain. ECGs were subsequently recorded continuously in conscious animals for approximately 7 days using the Ponemah Software (DSI Harvard Bioscience Inc.). Mice were kept at a stable temperature with a regular 12 h light/dark cycle. To exclude the effects of pain and anesthesia, continuous ECG recordings between days 5–7 post-lead implantations were only included in the analysis of mean heart rates.

Cold tolerance—Mice were acclimatized for at least 3 weeks at 26°C. Mice at 6–8 weeks of age were anesthetized with isoflurane, abdominal skin was shaved, and a 1.5 cm incision was made at the abdominal midline. Real-time readable temperature loggers (Anipill, Herouville, France) were implanted into the intraperitoneal cavity to a position ventral to the caudal arteries and veins but dorsal to the abdominal viscera. Abdominal musculature was closed with an absorbable suture (chromic gut 4/0; AD surgical) and the skin incision was with a non-absorbable nylon (Ethilon black 4/0; ProNorth Medical) suture. Analgesia (meloxicam 2 mg/kg) was provided subcutaneously for 2 days following surgery. After recovery for 10–12 days from surgery, mice were transferred to a 4°C cold cabinet for 4 h, where they were individually housed. Core body temperatures were recorded every 15 min using the AniLogger Monitor. Data were analyzed using GraphPad Prism 9.

Glucose-induced insulin secretion—Mice (6–8 weeks) were individually housed and fasted overnight (16 h). The next morning, mice were i.p. injected with 3 g/kg glucose/saline (Sigma-Aldrich). Tail blood was collected at the indicated time, spun down at 3000 rpm for 15 min, and plasma insulin levels were measured with an Ultrasensitive Insulin ELISA kit (Crystal Chem, Elk Grove Village, IL).

Mouse islet isolations, *in vitro* insulin secretion and insulin content—Islets were isolated from mice at 6–8 weeks of age. Briefly, islets were isolated by collagenase distension through the bile duct (Collagenase P [Roche, Basel, Switzerland], 0.375 mg/mL in HBSS) and digestion at 37°C.[84] Digested pancreata were washed with HBSS +0.1% BSA and subjected to discontinuous density gradient using histopaque (6:5 Histopaque 1119:1077; Sigma, St. Louis, MO). The islet layer (found at the interface) was collected and islets were handpicked under an inverted microscope for subsequent analysis. For insulin secretion in isolated islets, harvested islets were allowed to recover overnight in RPMI-1640 media containing 10% fetal bovine serum, and 5U/L penicillin/streptomycin (Invitrogen). Islets were washed with Krebs-Ringer HEPES buffer (KRBH) containing low (2.8 mM) glucose and pre-incubated for 1 h in low-glucose KRBH. After pre-incubation, groups of

similarly sized 14 islets were handpicked into a 24-well plate and allowed to incubate for 30 min in KRBH containing low glucose, or high (16.7 mM) glucose. After incubation the supernatant fractions were removed and the islets were lysed with acid ethanol, followed by ELISA to determine the insulin content in both supernatant and islet fractions. Insulin values were normalized to islet DNA content from the same lysates using a Picogreen Kit (Thermo Fisher Scientific).

Glucagon secretion—Mice (8 weeks) were individually housed and fasted for 6 h. Mice were injected with 0.75 U/kg of insulin (Novolin-R, Novo Nordisk, Princeton, NJ; i.p.). Tail blood was collected in microfuge tubes containing 2 μg/mL aprotinin at the indicated times, spun down at 3000 rpm for 15 min, and plasma glucagon levels were measured with a Glucagon 10 μL ELISA kit (Mercodia).

Glucose tolerance test—Mice (6–8 weeks) were individually housed and fasted overnight (16 h). The next morning, mice were i.p. injected with 2 g/kg glucose/saline (Sigma-Aldrich), and tail blood glucose levels were measured using OneTouch Ultra glucometer at the indicated time.

Insulin sensitivity test—Mice (6–8 weeks) were individually housed and fasted for 6 h before being i.p. injected 0.75 U/kg of insulin (Novolin-R, Novo Nordisk, Princeton, NJ). Tail blood glucose levels were measured using a OneTouch Ultra glucometer at indicated times.[85]

Pupil analyses—Pupil size measurements were performed as reported.[86] Mice were dark-adapted for over 2 h before the experiment. For all recordings, mice were un-anesthetized and restrained by hand. To mitigate stress, which can affect pupil size, researchers handled mice for several days prior to the experiments. A Sony Handycam (FDR-AX33), carrying a prime lens, set at manual focusing and night shot mode, accompanied by an external infrared light source, was used for recording. The dotted pattern from the infrared light source is reflected by the mouse cornea and used as the focusing indicator. The equipment ensures that mouse pupils can only be focused at a fixed distance from the camera and can be easily visualized in the dark. Pupil size was measured by the maximum diameter using Fiji software in each picture frame. To measure dark-adapted baseline pupil size, a 10 s video was recorded.

To examine parasympathetic activity, mice were dark-adapted as described above. Un-anesthetized mice were restrained by hand. To measure pupil responses to light, a video of 10 s in the dark followed by 30 s exposure to white light at 0.01, 0.1, 1, 10, 100, 1000 lux, respectively, were recorded. The pupil constriction is quantified by normalizing the pupil area at 30 s to the baseline area in the dark.

Neuronal counts—CG-SMGs were dissected from mice at P21, fixed in 4% PFA at 4°C for 4 h, and cryoprotected in 30% sucrose/PBS overnight. CG-SMGs were mounted in OCT and serially sectioned with 12 μm thickness. Every fifth section was stained with a solution containing 0.5% cresyl violet (Nissl).[83]. Cells in CG-SMGs with characteristic neuronal morphology and visible nucleoli were counted using ImageJ.

Immunohistochemical analyses—For SCG, and CG-SMG immunostaining, mice torsos at indicated ages were fixed in 4% PFA/PBS for 4 h to overnight and cryoprotected in 30% sucrose/PBS for 2–3 days. Target tissues from mice at postnatal day 6 or 21, were dissected and fixed in 4% PFA/PBS overnight and cryoprotected in 30% sucrose/PBS for 48 h. Torsos and target tissues were embedded in OCT (Sakura Finetek) and stored at −80°C. SCG, CG-SMG were cryo-sectioned at 14 μm while target tissues at 50 μm. For paraffin embedding, SCG and CG-SMG were fixed in Bouin's solution for 1 h at room temperature, washed, and left in 70% ethanol at room temperature, followed by dehydration with 50%, 75%, 85%, 95%, and 100% ethanol and xylene. Tissues were embedded in paraffin and sectioned at 6 μm using a microtome, deparaffinized using xylene, and rehydrated using 100%, 95%, 85%, 75%, and 50% ethanol. Paraffin sections were incubated in 10 mM sodium citrate buffer (pH 6) at 95°C for 10 min, followed by incubation in 0.2 M glycine for 10 min. Both cryo- and paraffin sections were then permeabilized in 1% Triton X-100 in PBS for 10 min at room temperature. Blocking was done in 10% goat or donkey serum/3% bovine serum albumin in 0.3% Triton X-100 in PBS for 1–2 h at room temperature. Primary antibodies used were rabbit/sheep/mouse anti-TH (1:300), rabbit anti-NPY (1:250), chicken anti-GFP (1:500), rabbit anti-RFP (1:500), with incubations overnight at 4°C. Slides were washed with 0.3% Triton X-100/PBS and incubated with Alexa 488, -546, or −647 conjugated anti-rabbit, anti-sheep, anti-mouse or anti-chicken secondary antibodies (1:400–500) in blocking solution for 1–2 h at room temperature. Tissues were then mounted in Aqueous Mounting Medium containing 100 μg/mL DAPI and imaged at 1 μm optical slices using a Zeiss LSM 700 or LSM 800 confocal scanning microscope. Maximum-intensity images were generated using ImageJ.

For cFos immunostaining, CG-SMG was dissected from mice that were kept at room temperature or exposed to cold (4°C, 1 h). Tissues were cryoprotected in 30% sucrose/PBS for 1 h at 4°C and embedded in OCT and stored at −80°C. 16 μm thick sections were prepared and fixed with 2% PFA/PBS for 5 min and permeabilized with freshly prepared 1% Triton X-100 for 15 min. Blocking was done in 5% goat serum/1% bovine serum albumin in 0.3% Triton X-100/PBS for 1.5 h at room temperature, followed by incubation with a polyclonal or monoclonal anti-rabbit cFos (1:1000) antibody diluted in blocking solution overnight at 4°C. After washes, sections were incubated in Alexa 546 conjugated anti-rabbit secondary antibody overnight at 4°C. Sections were mounted using ProLong Gold (Thermo Fisher) antifade mounting media and images were acquired using LSM 800 confocal scanning microscope.

iDISCO and wholemount immunostaining—iDISCO-based tissue clearing for whole mount immunostaining of sympathetic chain and target organs were performed in P6 mice.[87] Briefly, the sympathetic chain and organs were fixed in 4%PFA/PBS, dehydrated by methanol/water series (20–80%), and incubated overnight in 66% dichloromethane (DCM)/33% methanol. Tissues were bleached with 5% H_2O_2 in methanol at 4°C overnight, re-hydrated with methanol/PBS/0.2% Triton X-100 series (80–20%), and permeabilized first with 0.2%Triton X-100/PBS for 2 h followed by 3 overnight permeabilizations with 0.2% Triton X-100/20%DMSO/0.3M glycine in PBS. Tissues were incubated in blocking solution (0.2% Triton X-100/10% DMSO/6% Normal Goat/Sheep Serum in PBS) for 2

overnight and then incubated with rabbit/sheep-*anti*-TH (1:300) or rabbit anti-RFP (1:300) in 0.2% Tween 20/0.001% heparin/5% DMSO/3% Normal Goat/Sheep Serum in PBS at 37°C for 4 overnight. Samples were then washed with 0.2% Tween 20/0.001% heparin in PBS and incubated with anti-rabbit Alexa 546 or anti-sheep Alexa 647 secondary antibody (1:400) in 0.2% Tween 20/0.001% heparin/3% Normal Goat/Sheep Serum in PBS for 4 overnight. Tissues were extensively washed with 0.2% Tween 20/0.001% heparin in PBS and dehydrated in methanol. Tissues were cleared by successive washes in 66% DCM/33% methanol, 100% DCM and 100% Dibenzyl Ether. Tissues were imaged using a light-sheet microscope (LaVision BioTec Ultra Microscope II). Imaris software was used for 3D reconstructions of images.

For wholemount immunostaining of ganglia, SCG or CG-SMG were dissected from P6 mice and fixed with 4%PFA/PBS at 4°C for 4 h. Tissues were permeabilized using 0.2% Triton X-100/20%DMSO/0.3M glycine/PBS for 1 h at room temperature and blocked with 0.2% Triton X-100/10% DMSO/6% Normal Goat Serum at room temperature overnight. Tissues were then incubated with primary antibody anti-rabbit TH antibody (1:300) in 0.2% Tween 20/0.001% heparin/5% DMSO/3% Normal Goat Serum at room temperature, 2 overnight. Tissues were washed with 0.2% Tween 20/0.001% heparin/PBS extensively and incubated with anti-rabbit Alexa 647 secondary antibody (1:400) in 0.2% Tween 20/0.001% heparin/3% Normal Goat Serum/PBS at room temperature, 2 overnight. tdTomato fluorescence was visualized with endogenous expression. Tissues were mounted using Aqueous Mounting Medium and images were acquired using LSM 800 confocal microscope.

QUANTIFICATION AND STATISTICAL ANALYSIS

For practical reasons, analysis of soma-size measurements, and neuron numbers analysis were performed in a semi-blinded manner. The experimenter was aware of the genotypes prior to the experiment but performed each immunostaining and analyses without knowing the genotypes. All physiological analyses were performed in a blinded manner with the experimenter only keeping track of the ear tag numbers. All graphs and statistical analyses were performed using GraphPad Prism 9. Statistical significance was determined using an unpaired, two-tailed student t-test, and a two-way ANOVA test for more than one variable. All error bars are represented as the standard error of the mean (SEM).

Supplementary Material

Refer to Web version on PubMed Central for supplementary material.

ACKNOWLEDGMENTS

We thank Haiqing Zhao for helpful comments on the manuscript. We also thank Ivo Kalajzic (UConn Health) for the generous gift of the $NPY^{fl/fl}$ mice. We thank the JHU Integrated Imaging Center for assistance with microscopy. The graphical abstract was prepared using BioRender. This work was supported by NIH R01 awards, NS114478 and NS107342, to R.K.

REFERENCES

1. Scott-Solomon E, Boehm E, and Kuruvilla R (2021). The sympathetic nervous system in development and disease. Nat. Rev. Neurosci. 22, 685–702. [PubMed: 34599308]
2. Jänig W, and Häbler HJ (2000). Specificity in the organization of the autonomic nervous system: a basis for precise neural regulation of homeostatic and protective body functions. Prog. Brain Res. 122, 351–367. [PubMed: 10737070]
3. Ernsberger U, Deller T, and Rohrer H (2020). The diversity of neuronal phenotypes in rodent and human autonomic ganglia. Cell Tissue Res. 382, 201–231. [PubMed: 32930881]
4. Lundberg JM, Rudehill A, Sollevi A, Fried G, and Wallin G (1989). Co-release of neuropeptide Y and noradrenaline from pig spleen in vivo: importance of subcellular storage, nerve impulse frequency and pattern, feedback regulation and resupply by axonal transport. Neuroscience 28, 475–486. [PubMed: 2922111]
5. Ekblad E, Edvinsson L, Wahlestedt C, Uddman R, Håkanson R, and Sundler F (1984). Neuropeptide Y co-exists and co-operates with noradrenaline in perivascular nerve fibers. Regul. Pept. 8, 225–235. [PubMed: 6379758]
6. Lundberg JM, Terenius L, Hökfelt T, Martling CR, Tatemoto K, Mutt V, Polak J, Bloom S, and Goldstein M (1982). Neuropeptide Y (NPY)-like immunoreactivity in peripheral noradrenergic neurons and effects of NPY on sympathetic function. Acta Physiol. Scand. 116, 477–480. [PubMed: 6763452]
7. Whim MD (2006). Near simultaneous release of classical and peptide co-transmitters from chromaffin cells. J. Neurosci. 26, 6637–6642. [PubMed: 16775152]
8. Kalra SP, and Kalra PS (2004). NPY and cohorts in regulating appetite, obesity and metabolic syndrome: beneficial effects of gene therapy. Neuropeptides 38, 201–211. [PubMed: 15337372]
9. Zarjevski N, Cusin I, Vettor R, Rohner-Jeanrenaud F, and Jeanrenaud B (1993). Chronic intracerebroventricular neuropeptide-Y administration to normal rats mimics hormonal and metabolic changes of obesity. Endocrinology 133, 1753–1758. [PubMed: 8404618]
10. Alldredge B (2010). Pathogenic involvement of neuropeptides in anxiety and depression. Neuropeptides 44, 215–224. [PubMed: 20096456]
11. Loh K, Herzog H, and Shi YC (2015). Regulation of energy homeostasis by the NPY system. Trends Endocrinol. Metab. 26, 125–135. [PubMed: 25662369]
12. Tan CMJ, Green P, Tapoulal N, Lewandowski AJ, Leeson P, and Herring N (2018). The Role of Neuropeptide Y in Cardiovascular Health and Disease. Front. Physiol. 9, 1281. [PubMed: 30283345]
13. Walker P, Grouzmann E, Burnier M, and Waeber B (1991). The role of neuropeptide Y in cardiovascular regulation. Trends Pharmacol. Sci. 12, 111–115. [PubMed: 2053188]
14. Erickson JC, Clegg KE, and Palmiter RD (1996). Sensitivity to leptin and susceptibility to seizures of mice lacking neuropeptide Y. Nature 381, 415–421. [PubMed: 8632796]
15. Erickson JC, Hollopeter G, and Palmiter RD (1996). Attenuation of the obesity syndrome of ob/ob mice by the loss of neuropeptide Y. Science 274, 1704–1707. [PubMed: 8939859]
16. Lin S, Boey D, and Herzog H (2004). NPY and Y receptors: lessons from transgenic and knockout models. Neuropeptides 38, 189–200. [PubMed: 15337371]
17. Karl T, Duffy L, and Herzog H (2008). Behavioural profile of a new mouse model for NPY deficiency. Eur. J. Neurosci. 28, 173–180. [PubMed: 18616565]
18. Zhang L, Bijker MS, and Herzog H (2011). The neuropeptide Y system: pathophysiological and therapeutic implications in obesity and cancer. Pharmacol. Ther. 131, 91–113. [PubMed: 21439311]
19. Wahlestedt C, Edvinsson L, Ekblad E, and Håkanson R (1985). Neuropeptide Y potentiates noradrenaline-evoked vasoconstriction: mode of action. J. Pharmacol. Exp. Ther. 234, 735–741. [PubMed: 3928874]
20. Dahlöf C, Dahlöf P, and Lundberg JM (1985). enhancement of blood pressure increase upon alpha-adrenoceptor activation and direct pressor effects in pithed rats. Eur. J. Pharmacol. 109, 289–292. [PubMed: 2987001]

21. Lundberg JM, Pernow J, Tatemoto K, and Dahlöf C (1985). Pre- and postjunctional effects of NPY on sympathetic control of rat femoral artery. Acta Physiol. Scand. 123, 511–513. [PubMed: 3838851]
22. Håkanson R, Wahlestedt C, Ekblad E, Edvinsson L, Sundler F, and Neuropeptide Y (1986). coexistence with noradrenaline. Functional implications. Prog. Brain Res. 68, 279–287. [PubMed: 3550891]
23. Wahlestedt C, and Håkanson R (1986). Effects of neuropeptide Y (NPY) at the sympathetic neuroeffector junction. Can pre- and postjunctional receptors be distinguished? Med. Biol. 64, 85–88. [PubMed: 3018392]
24. Yu J, Xiao K, Chen X, Deng L, Zhang L, Li Y, Gao A, Gao J, Wu C, Yang X, et al. (2022). Neuron-derived neuropeptide Y fine-tunes the splenic immune responses. Neuron 110, 1327–1339.e6. [PubMed: 35139365]
25. Sharma S, Littman R, Tompkins JD, Arneson D, Contreras J, Dajani AH, Ang K, Tsanhani A, Sun X, Jay PY, et al. (2023). Tiered sympathetic control of cardiac function revealed by viral tracing and single cell transcriptome profiling. Elife 12, e86295. [PubMed: 37162194]
26. Furlan A, La Manno G, Lübke M, Häring M, Abdo H, Hochgerner H, Kupari J, Usoskin D, Airaksinen MS, Oliver G, et al. (2016). Visceral motor neuron diversity delineates a cellular basis for nipple- and pilo-erection muscle control. Nat. Neurosci. 19, 1331–1340. [PubMed: 27571008]
27. Liu S, Wang ZF, Su YS, Ray RS, Jing XH, Wang YQ, and Ma Q (2020). Somatotopic Organization and Intensity Dependence in Driving Distinct NPY-Expressing Sympathetic Pathways by Electroacupuncture. Neuron 108, 436–450.e7. [PubMed: 32791039]
28. Masliukov PM, Konovalov VV, Emanuilov AI, and Nozdrachev AD (2012). Development of neuropeptide Y-containing neurons in sympathetic ganglia of rats. Neuropeptides 46, 345–352. [PubMed: 22964363]
29. Milstein AD, Bloss EB, Apostolides PF, Vaidya SP, Dilly GA, Zemelman BV, and Magee JC (2015). Inhibitory Gating of Input Comparison in the CA1 Microcircuit. Neuron 87, 1274–1289. [PubMed: 26402609]
30. Srinivas S, Watanabe T, Lin CS, William CM, Tanabe Y, Jessell TM, and Costantini F (2001). Cre reporter strains produced by targeted insertion of EYFP and ECFP into the ROSA26 locus. BMC Dev. Biol. 1, 4. [PubMed: 11299042]
31. Myers AK, Farhat MY, Vaz CA, Keiser HR, and Zukowska-Grojec Z (1988). Release of immunoreactive-neuropeptide by rat platelets. Biochem. Biophys. Res. Commun. 155, 118–122. [PubMed: 3415675]
32. Yang K, Guan H, Arany E, Hill DJ, Cao X, and Neuropeptide Y (2008). is produced in visceral adipose tissue and promotes proliferation of adipocyte precursor cells via the Y1 receptor. FASEB. J. 22, 2452–2464. [PubMed: 18323405]
33. Baldock PA, Allison SJ, Lundberg P, Lee NJ, Slack K, Lin EJD, Enriquez RF, McDonald MM, Zhang L, During MJ, et al. (2007). Novel role of Y1 receptors in the coordinated regulation of bone and energy homeostasis. J. Biol. Chem. 282, 19092–19102. [PubMed: 17491016]
34. Rodnoi P, Rajkumar M, Moin ASM, Georgia SK, Butler AE, and Dhawan S (2017). Neuropeptide Y expression marks partially differentiated beta cells in mice and humans. JCI Insight 2, e94005. [PubMed: 28614797]
35. Madisen L, Garner AR, Shimaoka D, Chuong AS, Klapoetke NC, Li L, van der Bourg A, Niino Y, Egolf L, Monetti C, et al. (2015). Transgenic mice for intersectional targeting of neural sensors and effectors with high specificity and performance. Neuron 85, 942–958. [PubMed: 25741722]
36. Quach DH, Oliveira-Fernandes M, Gruner KA, and Tourtellotte WG (2013). A sympathetic neuron autonomous role for Egr3-mediated gene regulation in dendrite morphogenesis and target tissue innervation. J. Neurosci. 33, 4570–4583. [PubMed: 23467373]
37. Daigle TL, Madisen L, Hage TA, Valley MT, Knoblich U, Larsen RS, Takeno MM, Huang L, Gu H, Larsen R, et al. (2018). A Suite of Transgenic Driver and Reporter Mouse Lines with Enhanced Brain-Cell-Type Targeting and Functionality. Cell 174, 465–480.e22. [PubMed: 30007418]
38. Ahrén B (2000). Autonomic regulation of islet hormone secretion–implications for health and disease. Diabetologia 43, 393–410. [PubMed: 10819232]

39. Lundberg JM, Terenius L, Hökfelt T, and Goldstein M (1983). High levels of neuropeptide Y in peripheral noradrenergic neurons in various mammals including man. Neurosci. Lett. 42, 167–172. [PubMed: 6689363]
40. Renshaw D, and Hinson JP (2001). Neuropeptide Y and the adrenal gland: a review. Peptides 22, 429–438. [PubMed: 11287098]
41. Wolfensberger M, Forssmann WG, and Reinecke M (1995). Localization and coexistence of atrial natriuretic peptide (ANP) and neuropeptide Y (NPY) in vertebrate adrenal chromaffin cells immunoreactive to TH, DBH and PNMT. Cell Tissue Res. 280, 267–276. [PubMed: 7781024]
42. Wee NKY, Sinder BP, Novak S, Wang X, Stoddard C, Matthews BG, and Kalajzic I (2019). Skeletal phenotype of the neuropeptide Y knockout mouse. Neuropeptides 73, 78–88. [PubMed: 30522780]
43. Ransdell JL, Faust TB, and Schulz DJ (2010). Correlated Levels of mRNA and Soma Size in Single Identified Neurons: Evidence for Compartment-specific Regulation of Gene Expression. Front. Mol. Neurosci. 3, 116. [PubMed: 21119779]
44. Kwon CH, Luikart BW, Powell CM, Zhou J, Matheny SA, Zhang W, Li Y, Baker SJ, and Parada LF (2006). Pten regulates neuronal arborization and social interaction in mice. Neuron 50, 377–388. [PubMed: 16675393]
45. Lachance PED, Miron M, Raught B, Sonenberg N, and Lasko P (2002). Phosphorylation of eukaryotic translation initiation factor 4E is critical for growth. Mol. Cell Biol. 22, 1656–1663. [PubMed: 11865045]
46. Shi Z, Madden CJ, and Brooks VL (2017). Arcuate neuropeptide Y inhibits sympathetic nerve activity via multiple neuropathways. J. Clin. Invest. 127, 2868–2880. [PubMed: 28628036]
47. Baldock PA, Lin S, Zhang L, Karl T, Shi Y, Driessler F, Zengin A, Hörmer B, Lee NJ, Wong IPL, et al. (2014). Neuropeptide y attenuates stress-induced bone loss through suppression of noradrenaline circuits. J. Bone Miner. Res. 29, 2238–2249. [PubMed: 24535841]
48. Shi YC, Lau J, Lin Z, Zhang H, Zhai L, Sperk G, Heilbronn R, Mietzsch M, Weger S, Huang XF, et al. (2013). Arcuate NPY controls sympathetic output and BAT function via a relay of tyrosine hydroxylase neurons in the PVN. Cell Metab. 17, 236–248. [PubMed: 23395170]
49. Zukowska-Grojec Z, and Neuropeptide Y (1995). A novel sympathetic stress hormone and more. Ann. N. Y. Acad. Sci. 771, 219–233. [PubMed: 8597401]
50. Westfall TC, Carpentier S, Chen X, Beinfeld MC, Naes L, and Meldrum MJ (1987). Prejunctional and postjunctional effects of neuropeptide Y at the noradrenergic neuroeffector junction of the perfused mesenteric arterial bed of the rat. J. Cardiovasc. Pharmacol. 10, 716–722. [PubMed: 2450243]
51. Sheng M, and Greenberg ME (1990). The regulation and function of c-fos and other immediate early genes in the nervous system. Neuron 4, 477–485. [PubMed: 1969743]
52. Kvetnansky R, Weise VK, Thoa NB, and Kopin IJ (1979). Effects of chronic guanethidine treatment and adrenal medullectomy on plasma levels of catecholamines and corticosterone in forcibly immobilized rats. J. Pharmacol. Exp. Ther. 209, 287–291. [PubMed: 35604]
53. Wang Q, Wang M, and Whim MD (2013). Neuropeptide y gates a stress-induced, long-lasting plasticity in the sympathetic nervous system. J. Neurosci. 33, 12705–12717. [PubMed: 23904607]
54. Cavadas C, Céfai D, Rosmaninho-Salgado J, Vieira-Coelho MA, Moura E, Busso N, Pedrazzini T, Grand D, Rotman S, Waeber B, et al. (2006). Deletion of the neuropeptide Y (NPY) Y1 receptor gene reveals a regulatory role of NPY on catecholamine synthesis and secretion. Proc. Natl. Acad. Sci. USA 103, 10497–10502. [PubMed: 16798884]
55. Stanley BG, Leibowitz SF, and Neuropeptide Y (1984). stimulation of feeding and drinking by injection into the paraventricular nucleus. Life Sci. 35, 2635–2642. [PubMed: 6549039]
56. Guyenet PG (2006). The sympathetic control of blood pressure. Nat. Rev. Neurosci. 7, 335–346. [PubMed: 16760914]
57. Clarke JG, Davies GJ, Kerwin R, Hackett D, Larkin S, Dawbarn D, Lee Y, Bloom SR, Yacoub M, and Maseri A (1987). Coronary artery infusion of neuropeptide Y in patients with angina pectoris. Lancet 1, 1057–1059. [PubMed: 2883396]

58. Michalkiewicz M, Michalkiewicz T, Kreulen DL, and McDougall SJ (2001). Increased blood pressure responses in neuropeptide Y transgenic rats. Am. J. Physiol. Regul. Integr. Comp. Physiol. 281, R417–R426. [PubMed: 11448843]
59. Lin EE, Scott-Solomon E, and Kuruvilla R (2021). Peripheral Innervation in the Regulation of Glucose Homeostasis. Trends Neurosci. 44, 189–202. [PubMed: 33229051]
60. Skoglund G, Gross R, Ahrén B, and Loubatières-Mariani MM (1993). Different mechanisms are involved in neuropeptide Y-induced pancreatic vasoconstriction and inhibition of insulin secretion. Eur. J. Pharmacol. 236, 69–74. [PubMed: 8100529]
61. Imai Y, Patel HR, Hawkins EJ, Doliba NM, Matschinsky FM, and Ahima RS (2007). Insulin secretion is increased in pancreatic islets of neuropeptide Y-deficient mice. Endocrinology 148, 5716–5723. [PubMed: 17717054]
62. Teitelman G, Alpert S, Polak JM, Martinez A, and Hanahan D (1993). Precursor cells of mouse endocrine pancreas coexpress insulin, glucagon and the neuronal proteins tyrosine hydroxylase and neuropeptide Y, but not pancreatic polypeptide. Development 118, 1031–1039. [PubMed: 7903631]
63. Tan CL, and Knight ZA (2018). Regulation of Body Temperature by the Nervous System. Neuron 98, 31–48. [PubMed: 29621489]
64. McDougal DH, and Gamlin PD (2015). Autonomic control of the eye. Compr. Physiol. 5, 439–473. [PubMed: 25589275]
65. Zukowska-Grojec Z (1998). Neuropeptide Y: an adrenergic cotransmitter, vasoconstrictor, and a nerve-derived vascular growth factor. Adv. Pharmacol. 42, 125–128. [PubMed: 9327862]
66. Lundberg JM, Rudehill A, Sollevi A, and Hamberger B (1989). Evidence for co-transmitter role of neuropeptide Y in the pig spleen. Br. J. Pharmacol. 96, 675–687. [PubMed: 2566349]
67. Borden P, Houtz J, Leach SD, and Kuruvilla R (2013). Sympathetic Innervation during Development Is Necessary for Pancreatic Islet Architecture and Functional Maturation. Cell Rep. 4, 287–301. [PubMed: 23850289]
68. Herring N, Lokale MN, Danson EJ, Heaton DA, and Paterson DJ (2008). Neuropeptide Y reduces acetylcholine release and vagal bradycardia via a Y2 receptor-mediated, protein kinase C-dependent pathway. J. Mol. Cell. Cardiol. 44, 477–485. [PubMed: 17996892]
69. Jänig W (2014). Sympathetic nervous system and inflammation: a conceptual view. Auton. Neurosci. 182, 4–14. [PubMed: 24525016]
70. Matsumoto SG, Gruener RP, and Kreulen DL (1993). Neurotransmitter properties of guinea-pig sympathetic neurons grown in dissociated cell culture–I. Adult neurons. Neuroscience 57, 1135–1145. [PubMed: 7906016]
71. Rubin E (1985). Development of the rat superior cervical ganglion: initial stages of synapse formation. J. Neurosci. 5, 697–704. [PubMed: 2983046]
72. De Potter WP, Partoens P, Schoups A, Llona I, and Coen EP (1997). Noradrenergic neurons release both noradrenaline and neuropeptide Y from a single pool: the large dense cored vesicles. Synapse 25, 44–55. [PubMed: 8987147]
73. Hirsch D, and Zukowska Z (2012). NPY and stress 30 years later: the peripheral view. Cell. Mol. Neurobiol. 32, 645–659. [PubMed: 22271177]
74. van den Pol AN, Yao Y, Fu LY, Foo K, Huang H, Coppari R, Lowell BB, and Broberger C (2009). Neuromedin B and gastrin-releasing peptide excite arcuate nucleus neuropeptide Y neurons in a novel transgenic mouse expressing strong Renilla green fluorescent protein in NPY neurons. J. Neurosci. 29, 4622–4639. [PubMed: 19357287]
75. Solt VB, Brown MR, Kennedy B, Kolterman OG, and Ziegler MG (1990). Elevated insulin, norepinephrine, and neuropeptide Y in hypertension. Am. J. Hypertens. 3, 823–828. [PubMed: 2261148]
76. Jaakkola U, Kakko T, Seppälä H, Vainio-Jylhä E, Vahlberg T, Raitakari OT, and Kallio J (2010). The Leu7Pro polymorphism of the signal peptide of neuropeptide Y (NPY) gene is associated with increased levels of inflammatory markers preceding vascular complications in patients with type 2 diabetes. Microvasc. Res 80, 433–439. [PubMed: 20691708]

77. Chen J, Cheng M, Wang L, Zhang L, Xu D, Cao P, Wang F, Herzog H, Song S, and Zhan C (2020). A Vagal-NTS Neural Pathway that Stimulates Feeding. Curr. Biol. 30, 3986–3998.e5. [PubMed: 32822608]

78. Everitt BJ, Hökfelt T, Terenius L, Tatemoto K, Mutt V, and Goldstein M (1984). Differential co-existence of neuropeptide Y (NPY)-like immunoreactivity with catecholamines in the central nervous system of the rat. Neuroscience 11, 443–462. [PubMed: 6144080]

79. Sawchenko PE, Swanson LW, Grzanna R, Howe PR, Bloom SR, and Polak JM (1985). Colocalization of neuropeptide Y immunoreactivity in brainstem catecholaminergic neurons that project to the paraventricular nucleus of the hypothalamus. J. Comp. Neurol. 241, 138–153. [PubMed: 3840810]

80. Sahu A, Kalra SP, Crowley WR, and Kalra PS (1988). Evidence that NPY-containing neurons in the brainstem project into selected hypothalamic nuclei: implication in feeding behavior. Brain Res. 457, 376–378. [PubMed: 3219564]

81. Vähätalo LH, Ruohonen ST, Mäkelä S, Kovalainen M, Huotari A, Mäkelä KA, Määttä JA, Miinalainen I, Gilsbach R, Hein L, et al. (2015). Neuropeptide Y in the noradrenergic neurones induces obesity and inhibits sympathetic tone in mice. Acta Physiol. 213, 902–919.

82. Tseng CJ, Mosqueda-Garcia R, Appalsamy M, and Robertson D (1989). Cardiovascular effects of neuropeptide Y in rat brainstem nuclei. Circ. Res. 64, 55–61. [PubMed: 2909302]

83. Mapps AA, Boehm E, Beier C, Keenan WT, Langel J, Liu M, Thomsen MB, Hattar S, Zhao H, Tampakakis E, and Kuruvilla R (2022). Satellite glia modulate sympathetic neuron survival, activity, and autonomic function. Elife 11, e74295. [PubMed: 35997251]

84. Wollheim CB, Meda P, and Halban PA (1990). Isolation of pancreatic islets and primary culture of the intact microorgans or of dispersed islet cells. Methods Enzymol. 192, 188–223. [PubMed: 1963663]

85. Ceasrine AM, Lin EE, Lumelsky DN, Iyer R, and Kuruvilla R (2018). Adrb2 controls glucose homeostasis by developmental regulation of pancreatic islet vasculature. Elife 7, e39689. [PubMed: 30303066]

86. Keenan WT, Rupp AC, Ross RA, Somasundaram P, Hiriyanna S, Wu Z, Badea TC, Robinson PR, Lowell BB, and Hattar SS (2016). A visual circuit uses complementary mechanisms to support transient and sustained pupil constriction. Elife 5, e15392. [PubMed: 27669145]

87. Scott-Solomon E, and Kuruvilla R (2020). Prenylation of Axonally Translated Rac1 Controls NGF-Dependent Axon Growth. Dev. Cell 53, 691–705.e7. [PubMed: 32533921]

Highlights

- NPY^{+} sympathetic neurons are more abundant in prevertebral vs. paravertebral ganglia
- Loss of sympathetic-derived NPY elevates heart rate but maintains blood pressure
- NPY cKO mice show impaired glucose tolerance and reduced insulin secretion
- NPY cKO mice show decreased cold tolerance

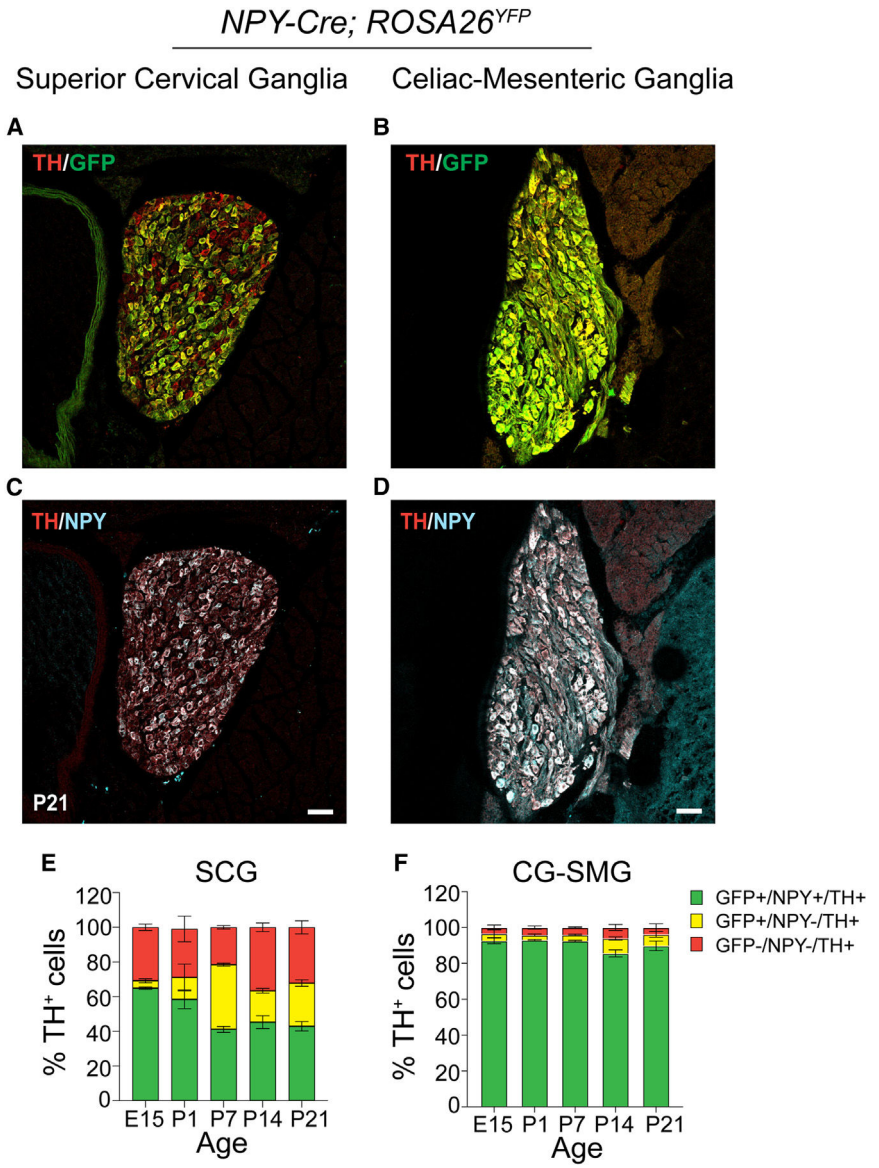

Figure 1. Differential NPY expression in paravertebral and prevertebral sympathetic neurons

(A–D) Immunostaining for TH, NPY, and GFP in superior cervical ganglia (SCGs; paravertebral) (A and C) and celiac-superior mesenteric ganglia (CG-SMGs; prevertebral) (B and D) in NPY-Cre:*ROSA26*^{EYFP} reporter mice.

(E and F) Percentage of NPY-expressing noradrenergic neurons in SCGs (E) and CG-SMGs (F). NPY and TH are co-expressed (green bar) in ~65% of SCG neurons at E15 and down-regulated to ~43% at P21. NPY and TH are co-expressed in ~90% of CG-SMG neurons throughout development. Neurons that expressed NPY earlier but no longer do so at the time of examination are represented by the yellow bars. Sympathetic neurons that never express NPY are indicated by red bars. n = 3 mice per genotype for each time point. Scale bars, 50 μm.

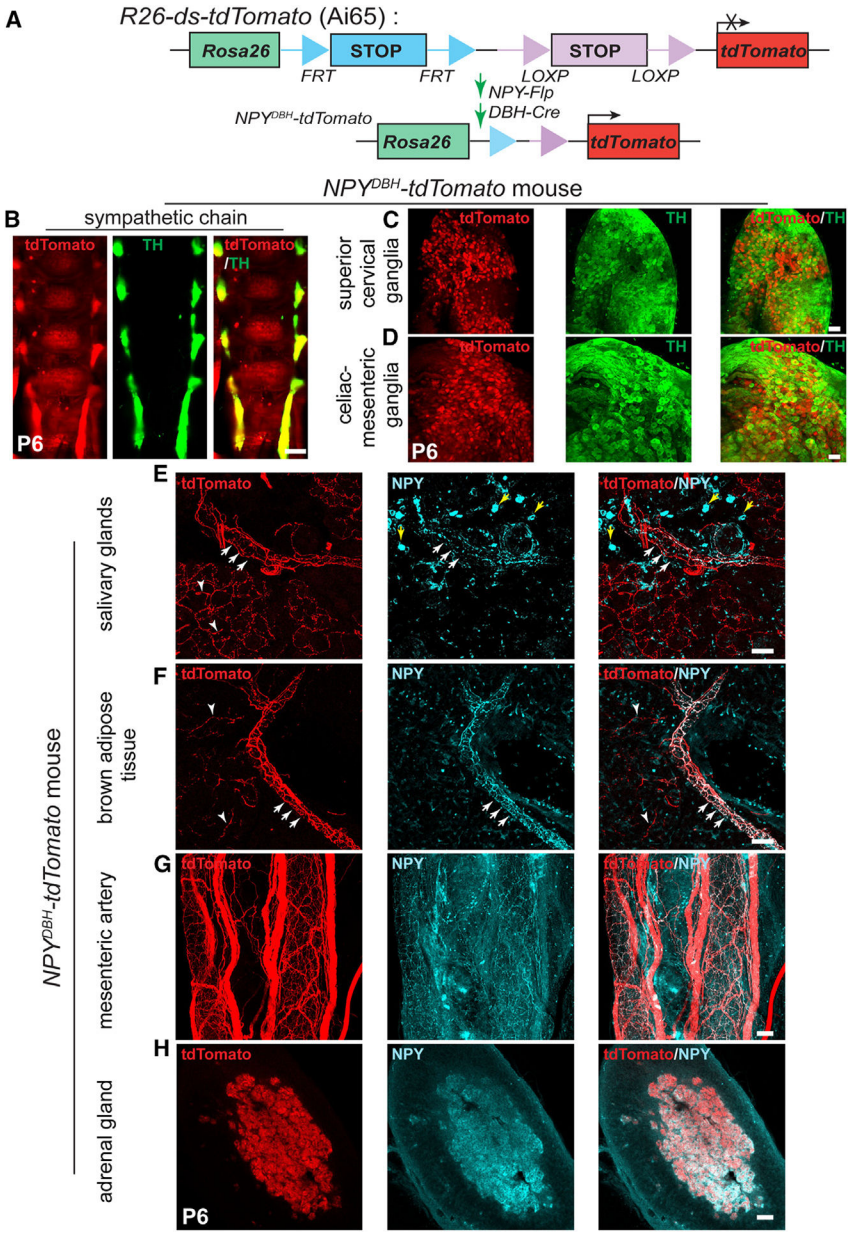

Figure 2. NPY-expressing sympathetic axons primarily innervate blood vessels

(A) Schematic showing the intersectional genetic strategy to generate *NPY^{DBH}-tdTomato* mice, where tdTomato expression is activated by removal of two *STOP* cassettes by Flpo and Cre recombinases in sympathetic neurons co-expressing NPY and DBH.

(B–D) Co-localization of tdTomato and TH in sympathetic chain (B), SCGs (C), or CG-SMGs (D) using whole-mount immunostaining in *NPY^{DBH}-tdTomato* mice at P6. Scale bars, 500 μm (B) and 100 μm (C and D).

(E and F) Innervation of paravertebral targets (salivary glands, BAT) by NPY^{DBH}-tdTomato sympathetic fibers. tdTomato signal (red) is observed in axons aligned with blood vessels (white arrows) as well as in tissue parenchyma (white arrowheads). Compared to reporter expression, axonal NPY immunostaining (cyan) is only found in axons associated with

vasculature. Yellow arrows indicate NPY immunostaining in non-neuronal cells. Scale bar, 50 μm.

(G and H) Co-localization of NPY protein and tdTomato reporter expression in mesenteric artery (prevertebral sympathetic target, G) and adrenal chromaffin cells (H). Scale bar, 50 μm.

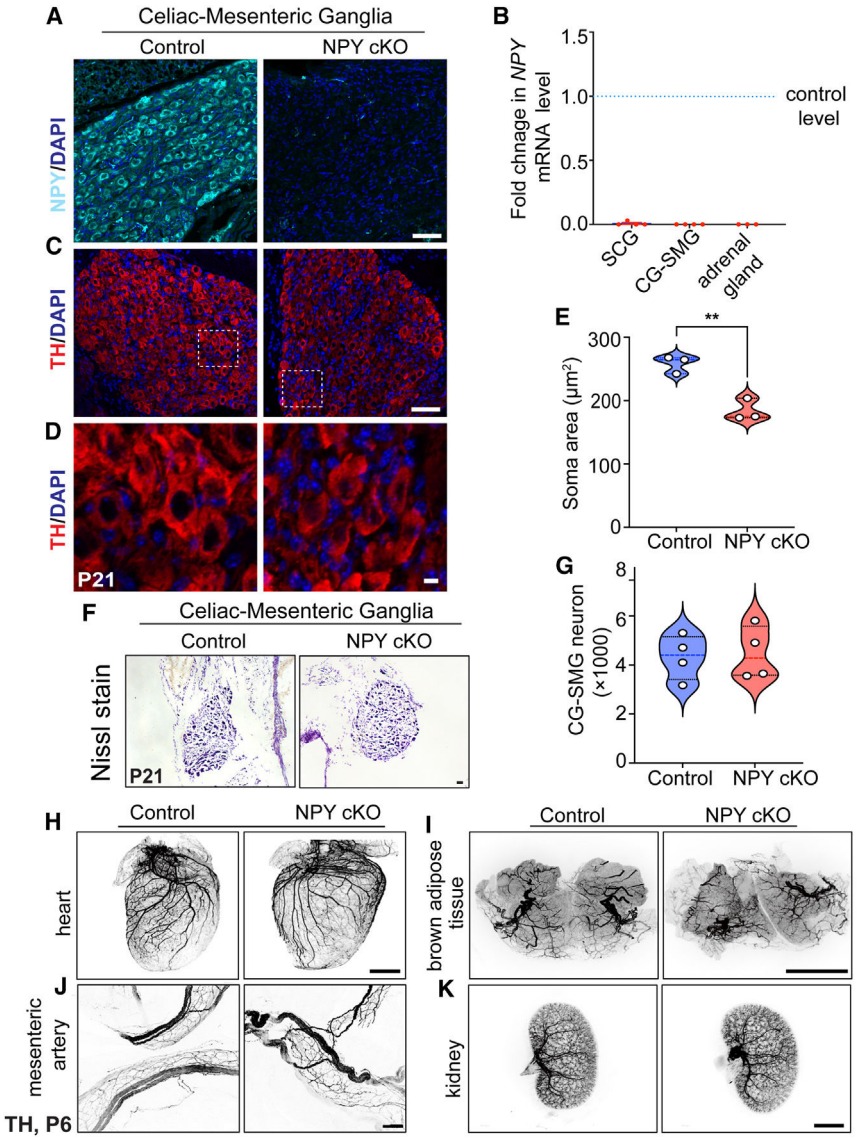

Figure 3. Loss of NPY in sympathetic neurons does not affect neuron survival and target innervation but results in reduced soma size

(A) Immunostaining shows a marked reduction in NPY protein in CG-SMGs from NPY cKO mice compared to control mice. Scale bar, 50 µm.

(B) qPCR analyses show a loss of *Npy* transcript in SCGs, CG-SMGs, and adrenal glands from NPY cKO mice. Results are means ± SEM from n = 4 animals per genotype for SCGs and CG-SMGs and n = 3 animals per genotype for adrenal glands.

(C and D) TH expression appears unaffected by NPY loss as shown by immunofluorescence.

(D) shows higher-magnification views of the insets in (C). Scale bars, 50 µm for (C) and 5 µm for (D).

(E) Quantification of soma areas from CG-SMG tissue sections shows that neuronal soma size is reduced in NPY cKO sympathetic ganglia. Results are means ± SEM from n = 3 mice per genotype. **p < 0.01; unpaired t test.

(F) Nissl staining of CG-SMGs in control and NPY cKO mice. Scale bar, 50 μm.
(G) Quantification of Nissl-stained neurons shows that neuron numbers are comparable between control and mutant mice. Results are means ± SEM from n = 4 per genotype.
(H–K) Whole-organ TH immunostaining imaged by light-sheet microscopy shows that sympathetic axon innervation of target tissues including the heart, BAT, mesenteric arteries, and kidneys is comparable between NPY cKO and control mice. Scale bars, mesenteric arteries: 50 μm; heart and kidney: 800 μm; and BAT: 1,500 μm.

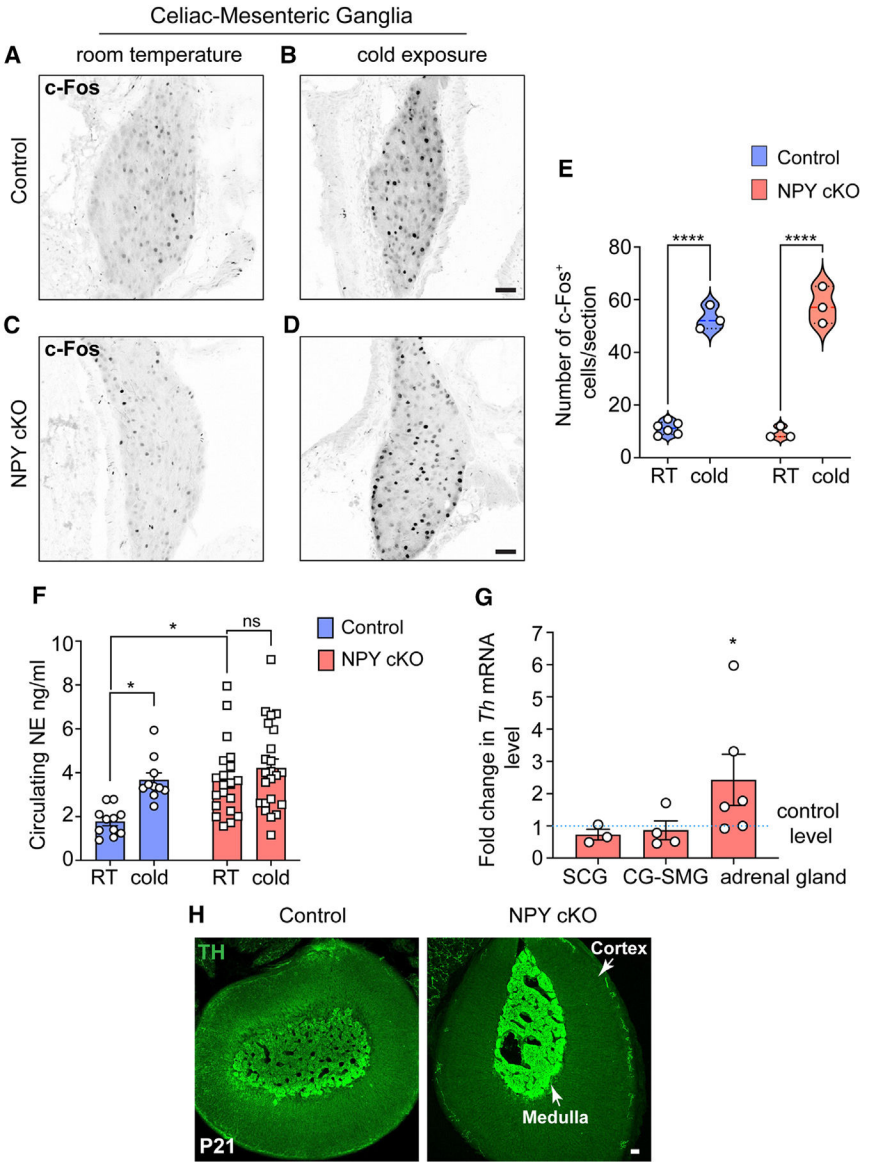

Figure 4. Loss of sympathetic NPY enhances circulating NE without affecting neuron activity

(A–D) Similar numbers of c-Fos-positive sympathetic neurons in the CG-SMG from 6- to 8-week-old control and NPY cKO mice housed at room temperature (RT; 26°C). Cold exposure (4°C, 1 h) increases the number of c-Fos-positive sympathetic neurons in both control and mutant ganglia. Scale bars, 50 μm.

(E) Quantification of c-Fos-positive sympathetic neurons in control and mutant CG-SMGs at RT and in response to cold exposure (4°C, 1 h). Data are presented as means ± SEM from n = 6 animals for control mice at RT and from n = 3 animals for all other conditions. ****$p < 0.0001$; two-way ANOVA, Tukey's multiple comparison test.

(F) Plasma NE levels are significantly elevated in NPY cKO mice compared to control animals at RT (26°C). Cold exposure (4°C, 2 h) significantly increases circulating NE in control, but not NPY cKO, animals. Data are as means ± SEM. n = 11 control and 20 mutant mice. *$p < 0.05$; two-way ANOVA, Tukey's multiple comparisons.

(G) *Th* mRNA is increased in adrenal glands, but not in sympathetic ganglia, in NPY cKO mice relative to control animals as shown by qPCR analysis. Results are means ± SEM from n = 3 mice per genotype for SCGs, 4 for CG-SMGs, and 6 for the adrenal glands. *$p < 0.05$; one-sample t test.

(H) TH immunofluorescence is increased in adrenal chromaffin cells in NPY cKO mice relative to control animals, indicating an increase in TH protein level. Scale bar, 50 μm.

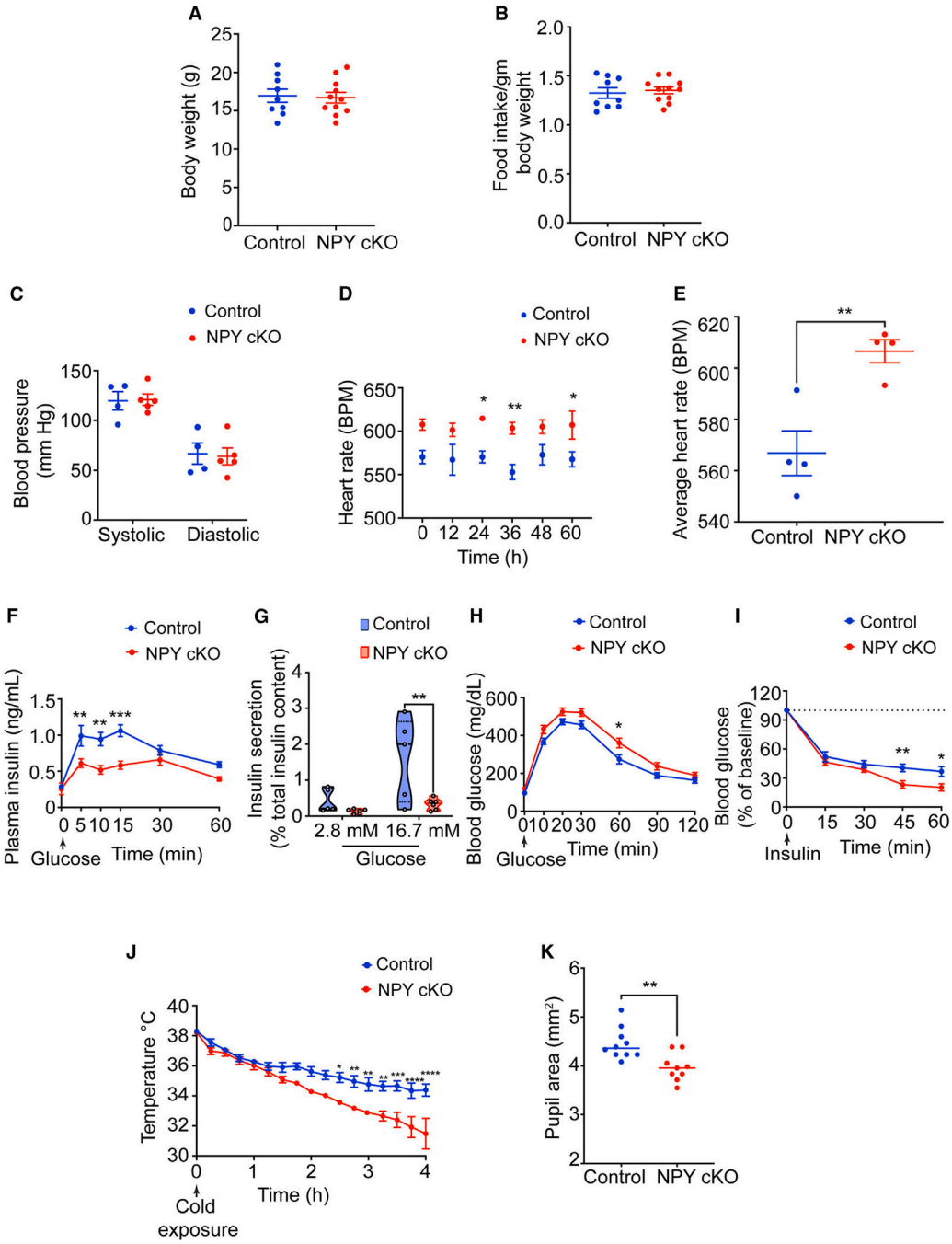

Figure 5. NPY cKO mice show metabolic and cardiovascular defects

(A and B) Body weight (A) and food intake (B) are comparable between NPY cKO and control mice. Results are means ± SEM from n = 9 control and 11 mutant mice; unpaired t test.

(C) Systolic and diastolic blood pressures are normal in NPY cKO mice. Results are means ± SEM from n = 4 control and 5 mutant mice; unpaired t test.

(D and E) NPY cKO mice show elevated heart rate compared to control animals. ECGs were recorded continuously in conscious mice for 7 days. To avoid confounding effects from

anesthesia, ECGs from days 5–7 were included in the analysis. Results are presented as means ± SEM from n = 4 mice per genotype. *p < 0.05 and **p < 0.01; two-way ANOVA, Sidak's multiple comparisons tests for (D) and unpaired t test for (E).

(F) NPY cKO mice show reduced plasma insulin levels in response to a glucose challenge (intraperitoneal [i.p.] injection of 3 g/kg glucose after 16 h fast) compared to control mice. Results are means ± SEM from n = 12 control and 8 mutant mice. **p < 0.01 and ***p < 0.001; two-way ANOVA, Sidak's multiple comparisons tests.

(G) Glucose-stimulated insulin secretion is reduced in isolated islets from NPY cKO mice relative to control animals. Islets were isolated from n = 5 control and 6 mutant mice. **p < 0.01; two-way ANOVA, Tukey's multiple comparisons tests.

(H) NPY cKO mice show impaired glucose tolerance. Results are means ± SEM from n = 12 control and 17 mutant mice. *p < 0.05; two-way ANOVA, Sidak's multiple comparisons tests.

(I) Improved insulin sensitivity in NPY cKO mice compared to control animals. Data are means ± SEM from n = 7 control and 6 mutant mice. *p < 0.05 and **p < 0.01; two-way ANOVA, Sidak's multiple comparisons tests.

(J) NPY cKO mice show impaired cold tolerance compared to control animals. Body temperatures were first recorded at RT (~26°C), after which mice were moved to 4°C and body temperatures were measured every 15 min for 4 h. Results are mean ± SEM from n = 5 mice per genotype. *p < 0.05, **p < 0.01, ***p < 0.001, and ****p < 0.0001; two-way ANOVA, Sidak's multiple comparisons tests.

(K) Dark-adapted NPY cKO mice have decreased basal pupil area compared to control mice. n = 10 control and 9 mutant mice. **p < 0.01; unpaired t test.

KEY RESOURCES TABLE

REAGENT or RESOURCE	SOURCE	IDENTIFIER
Antibodies		
Rabbit polyclonal anti-NPY	BMA Biomedicals	(Cat# T-4070, RRID:AB_518504)
Chicken polyclonal anti-GFP	Abcam	(Cat# ab13970, RRID:AB_300798)
Rabbit polyclonal anti-tyrosine hydroxylase	Millipore	(Cat# ab152, RRID:AB_390204)
Mouse monoclonal anti-tyrosine hydroxylase	Sigma-Aldrich	(Cat# T2928, RRID:AB_477569)
Sheep polyclonal anti-tyrosine hydroxylase	Millipore	(Cat# ab1542, RRID:AB_90755)
Rabbit monoclonal anti-RFP	Abcam	(Cat# ab185921, RRID:AB_2934052)
Rabbit polyclonal anti-cFos	Abcam	(Cat# ab190289; RRID:AB_2737414)
Rabbit monoclonal anti-cFos	Abcam	(Cat# ab222699, RRID:AB_2891049)
Donkey anti-Rabbit IgG Alexa Flour 647	Thermo Fisher Scientific	(Cat# A-31573, RRID:AB_2536183)
Donkey anti-Chicken IgG Alexa Flour 488	Sigma-Aldrich	(Cat# SAB4600031, RRID:AB_2721061)
Donkey anti-Sheep IgG Alexa Flour 546	Thermo Fisher Scientific	(Cat# A-21098, RRID:AB_2535752)
Donkey anti-Sheep IgG Alexa Flour 647	Abcam	(Cat# ab150179, RRID:AB_2884038)
Goat anti-Mouse IgG1 Alexa 647	Thermo Fisher Scientific	(Cat# A-21240, RRID:AB_2535809)
Goat anti-Rabbit IgG Alexa 647	Thermo Fisher Scientific	(Cat# A-21244, RRID:AB_2535812)
Goat anti-Rabbit IgG Alexa 546	Thermo Fisher Scientific	(Cat# A-11035, RRID:AB_2534093)
Chemicals, peptides, and recombinant proteins		
Glycogen, RNA grade	Thermo Fisher Scientific	Cat# R0551
Trizol	Thermo Fisher Scientific	Cat# 15596018
Maxima SYBR Green/ROX qPCR Master Mix (2X)	Thermo Fisher Scientific	Cat# K0222
Paraformaldehyde, reagent grade	Sigma-Aldrich	Cat# P6148-500G
Bouin’s solution	Sigma-Aldrich	Cat# HT10132- 1L
DAPI	Roche	Cat# 10236276001
ProLong Gold Antifade Mountant	Thermo Fisher Scientific	Cat# P36930
Fluoromount Mounting Media	Sigma-Aldrich	Cat# F4680- 25mL
Permount Mounting Media	Fisher Scientific	Cat# SP11500
Hydrogen peroxide solution, 30%in H2O, ACS reagent	Sigma-Aldrich	Cat# 216763
Heparin sodium salt	Sigma-Aldrich	Cat# H3393
Isoflurane	MWI	Cat# 502017
Insulin	Novolin-R	Cat# A10005804
D-(+)-Glucose, ACS reagent	Sigma-Aldrich	Cat# G5767-25G
Histopaque(R)-1077	Sigma-Aldrich	Cat#10771
Histopaque(R)-1119	Sigma-Aldrich	Cat#11191

REAGENT or RESOURCE	SOURCE	IDENTIFIER
Collagenase P	Sigma-Aldrich	Cat#11249002001
Aprotinin	Sigma-Aldrich	Cat#A1153
Critical commercial assays		
Superscript IV First Strand Synthesis System	Thermo Fisher Scientific	Cat# 18091050
Ultra-Sensitive Mouse Insulin ELISA Kit	Crystal Chem	Cat# 90080
PicoGreen Kit	Thermo Fisher Scientific	Cat#P7581
Norepinephrine High Sensitive ELISA Kit	Rocky Mountain Diagnostics	Cat# BA E–5200R
Mercodia Glucagon 10ul ELISA	Mercodia	Cat#10-1281-01
Experimental models: Organisms/strains		
Mouse: *B6.Cg-Npytm1(cre)Zman/J*	The Jackson Laboratory	RRID:IMSR_JAX:027851
Mouse: *B6.129X1-Gt(ROSA)26Sortm1(EYFP)Cos/J*	The Jackson Laboratory	RRID:IMSR_JAX:006148
Mouse: *DBH-Cre*	Quach et al.[36]	N/A
Mouse: *B6.Cg-Npytm1.1(flpo)Hze/J*	The Jackson Laboratory	RRID:IMSR_JAX:030211
Mouse: *B6;129S-Gt(ROSA)26Sortm65.1(CAG-tdTomato)Hze/J*	The Jackson Laboratory	RRID:IMSR_JAX:021875
Mouse: $NPY^{fl/fl}$	Wee et al.[42]	N/A
Mouse: *C57Bl/6J* (Strain background)	The Jackson Laboratory	RRID:IMSR_JAX:000664
Oligonucleotides		
*Npy*_F:5′-AGAGATCCAGCCCTGAGACA-3′	This paper	qPCR primers
*Npy*_R:5′-GATGAGGGTGGAAACTTGGA-3′	This paper	qPCR primers
*Th*_F:5′-AATCCACCACTTAGAGACCCG	This paper	qPCR primers
*Th*_R:3′-CTTGGTGACCAGGTGGTGAC	This paper	qPCR primers
*18s*_F:5′-CGCCGCTAGAGGTGAAATTC	This paper	qPCR primers
*18s*_R:5′-TTGGCAAATGCTTTCGCTC	This paper	qPCR primers
*Npyfl/fl*_F:5′-GCCTCCGTGCCTCTTATCTT-3′	Wee et al.[42]	Genotyping primers
*Npyfl/fl*_R:5′-GATTTTGGAGGCAACAGAGC-3′	Wee et al.[42]	Genotyping primers
*B6.Cg-Npytm1(cre)Zman/J*_F: 5′-TCC ATG ATT TGC CTC TTG TG -3′	The Jackson Laboratory	Genotyping primers
*B6.Cg-Npytm1(cre)Zman/J*_R: 5′-ACA CCG GCC TTA TTC CAA G -3′	The Jackson Laboratory	Genotyping primers
*B6.129X1-Gt(ROSA)26Sortm1(EYFP)Cos/J*_F: 5′-AGG GCG AGG AGC TGT TCA-3′	The Jackson Laboratory	Genotyping primers
*B6.129X1-Gt(ROSA)26Sortm1(EYFP)Cos/J*_R: 5′-TGA AGT CGA TGC CCT TCA G -3′	The Jackson Laboratory	Genotyping primers
*DBH-Cre*_F:5′-CTG CCA GGG ACA TGG CCA GG-3′	Quach et al.[36]	Genotyping primers
*DBH-Cre*_R:5′- GCA CAG TCG AGG CTG ATC AGC -3′	Quach et al.[36]	Genotyping primers
*B6.Cg-Npytm1.1(flpo)Hze/J*_F: 5′-TGC TGC TGT TCT CCG TAG C-3′	The Jackson Laboratory	Genotyping primers
*B6.Cg-Npytm1.1(flpo)Hze/J*_R: 5′-ACA CCG GCC TTA TTC CAA G-3′	The Jackson Laboratory	Genotyping primers

REAGENT or RESOURCE	SOURCE	IDENTIFIER
*B6;129S-Gt(ROSA)26Sortm65.1(CAG-tdTomato)Hze/J*_F:5′-CTG TTC CTG TAC GGC ATG G-3′	The Jackson Laboratory	Genotyping primers
*B6;129S-Gt(ROSA)26Sortm65.1(CAG-tdTomato)Hze/J*_R:5′-GGC ATT AAA GCA GCG TAT CC -3′	The Jackson Laboratory	Genotyping primers
Software and algorithms		
Ponemah Software	N/A	https://www.datasci.com/products/software/ponemah
Anilogger Manager software	N/A	https://www.animals-monitoring.fr/wp-content/uploads/2020/06/P120GUI004-Quick.Start_.Anilogger.system.EN_.pdf
Imaris	Oxford	https://imaris.oxinst.com
ImageJ	N/A	https://ImageJ.nih.gov/ij/
ZEN 2012 (blue edition)	N/A	https://www.zeiss.com/microscopy/int/home.html
GraphPad Prism9	N/A	https://www.graphstats.net/graphpad-prism
BioRender	N/A	www.biorender.com